Earth System
Dynamics
Discussions

Open Access

EGU

The ExtremeX global climate model experiment: Investigating thermodynamic and dynamic processes contributing to weather and climate extremes

Kathrin Wehrli[1], Fei Luo[2,3], Mathias Hauser[1], Hideo Shiogama[4], Daisuke Tokuda[5], Hyungjun Kim[5], Dim Coumou[2,3], Wilhelm May[6], Philippe Le Sager[3], Frank Selten[3], Olivia Martius[7,8,9], Robert Vautard[10], and Sonia I. Seneviratne[1]

[1]Institute for Atmospheric and Climate Science, Department of Environmental Systems Science, ETH Zurich, Zurich, Switzerland
[2]Institute for Environmental Studies, VU University Amsterdam, Amsterdam, Netherlands
[3]Royal Netherlands Meteorological Institute (KNMI), De Bilt, Netherlands
[4]Center for Global Environmental Research, National Institute for Environmental Studies, Tsukuba, Japan
[5]Institute of Industrial Science, University of Tokyo, Tokyo, Japan
[6]Centre for Environmental and Climate Science (CEC), Lund University, Lund, Sweden
[7]Oeschger Centre for Climate Change Research, University of Bern, Bern, Switzerland
[8]Institute of Geography, University of Bern, Bern, Switzerland
[9]Mobiliar Lab for Natural Risks, University of Bern, Bern, Switzerland
[10]Institut Pierre Simon Laplace, Laboratoire des Sciences du Climat et de l'Environnement (LSCE), Gif sur Yvette, France

Correspondence: Kathrin Wehrli (kathrin.wehrli@env.ethz.ch)

Abstract. The mechanisms leading to the occurrence of extreme weather and climate events are varied and complex. They generally encompass a combination of dynamical and thermodynamical processes, as well as drivers external to the climate system, such as anthropogenic greenhouse gas emissions and land-use change. Here we present the ExtremeX multi-model intercomparison experiment, which was designed to investigate the contribution of dynamic and thermodynamic processes to recent weather and climate extremes. The numerical experiments are performed with three Earth System Models: CESM, MIROC, and EC-Earth. They include control experiments with interactive atmosphere and land surface conditions, and experiments where either the atmospheric circulation, soil moisture or both are constrained using observation-based values. The temporal evolution and magnitude of temperature anomalies during heatwaves is well represented in the experiments with constrained atmosphere. However, mean climatological biases in temperature and precipitation are not substantially reduced in any of the constrained experiments, highlighting the importance of error compensations and tuning in the standard model versions. The results further reveal that both atmospheric circulation patterns and soil moisture conditions substantially contribute to the occurrence of heat extremes. Soil moisture effects are particularly important in the tropics, the monsoon areas and the Great Plains of the United States.

1 Introduction

Weather and climate extremes strongly affect society, human health, and ecosystems; therefore they need to be accurately simulated in numerical weather predictions and climate projections (e.g. Seneviratne et al., 2012). However, substantial biases remain in their representation in weather and climate models (e.g. Angélil et al., 2016; Maraun et al., 2017; Merz et al., 2020; Moon et al., 2018; Wehrli et al., 2018). Across climate models of the fifth phase of the Coupled Model Intercomparison Project (CMIP5) consistent biases can be found in the mean climatology of the lower atmosphere and land surface, for example temperature and precipitation (Flato et al., 2013; Mueller and Seneviratne, 2014). These biases originate to some extent from the representation of the underlying processes driving evapotranspiration at the land surface (Mueller and Seneviratne, 2014), extratropical cyclones (Zappa et al., 2013), or the simulated sea ice and sea surface temperatures (SSTs) (Turner et al., 2013; Wang et al., 2014). The difficulties in representing the mean climatology translate to biases in the representation of extreme events and impede their projection into the future. Therefore, an important question in the investigation of changes in extremes in a warming climate is the identification of the respective contribution of thermodynamic (thermal structure, water vapor and precipitation, land-atmosphere interactions) and dynamic (large-scale circulation) processes to their changes in occurrence and intensity (e.g. Pfahl et al., 2017; Shepherd, 2014; Trenberth et al., 2015; Wehrli et al., 2018, 2019; Zappa et al., 2015). Better isolating these contributions would help inform further model development as well as research on the attribution and projection of changes in weather and climate extremes (Vautard et al., 2016).

In the past, the number of record-breaking hot extremes has increased and it is expected to increase further if anthropogenic emissions continue to rise (e.g. Rahmstorf and Coumou, 2011; Shiogama et al., 2016; Power and Delage, 2019). Changes in the frequency, intensity and duration of various types of extremes can be seen in different regions of the world (e.g. Seneviratne et al., 2012). The most extreme events show the highest sensitivity to climate change (Seneviratne et al., 2014; Sillmann et al., 2013) and new, yet unseen, extreme intensities are appearing. These changes follow from a number of physical processes, their interactions with each other and their response to climate change.

In this study, we present the new "ExtremeX" multi-model experiment in which the contribution of thermodynamic and dynamic processes to recent extreme events is investigated in three Earth System Models (ESMs). The models used in ExtremeX are the Community Earth System Model version 1.2 (CESM1.2), the Model for Interdisciplinary Research on Climate version 5 (MIROC5) and the European Community Earth System Model version 3 (EC-Earth3). The ExtremeX experiment builds on the study of Wehrli et al. (2019) and investigates the contribution of atmospheric circulation patterns vs. soil moisture conditions for extreme weather and climate events between 2010 to 2015. The experiments are carried out with prescribed (SSTs) and sea ice and additionally constraining the land surface and/ or the atmosphere using observation-based conditions. The atmospheric variability is constrained using a grid-point nudging approach (Jeuken et al., 1996), which relaxes the dynamical model variables toward a given meteorological field. Droughts and land-based heatwaves are often also associated to soil moisture scarcity, especially in transitional climate zones due to the strong land-atmosphere coupling (e.g. Seneviratne et al., 2010; Zscheischler and Seneviratne, 2017). To control the role of land surface feedbacks on extreme events, soil moisture in the upper soil columns is constrained through either a nudging or a prescription method (depending on model implementation).

The presented work expands on previous work in Wehrli et al. (2018, 2019) by validating the forcing of the atmosphere and the land for the near-surface climatology. Near-surface temperature anomalies during four heatwaves evaluated in Wehrli et al. (2019) are compared in the three ESMs of ExtremeX. Additionally, warm spells are examined grid-point wise to identify the role of the atmosphere and soil moisture for different spell lengths. The research questions asked in the following are:

50

– Are model deficiencies in atmospheric circulation and the land surface contributing to overall model biases? Are model biases reduced when these processes are constrained?

– Are the ExtremeX ESMs able to reproduce temperature anomalies of past heatwaves when constrained with observations?

55

– What is the role of the physical climate drivers and climate change for four observed heatwaves?

– What is the relative contribution of the land surface and the atmospheric circulation to warm spells globally and how do the contributions vary regionally?

2   Design of the model intercomparison project

60   The ExtremeX experiment was conducted in a collaboration of three modeling groups running three ESMs, whereof two (CESM and MIROC) were run in the CMIP5 configuration and one (EC-Earth) in the CMIP6 configuration. Five experiments were designed to tackle the source of model biases and to separate the contribution of atmospheric circulation and land surface conditions to extreme events. This is done by constraining the ocean, land surface and atmosphere using observation-based values. The experiments and methods used are described in the following. They overall follow the setup of Wehrli et al. (2019).

2.1   Experimental design

65

Five experiments are included in ExtremeX. All experiments prescribe SSTs, sea ice and vegetation but differ in the simulation of the atmospheric circulation and soil moisture that are either interactive or prescribed. See Table 1 for an overview of the experiments. The control experiment (AI_SI, "Atmosphere Interactive, Soil Interactive") uses the standard setup where the atmosphere and soil moisture are both interactive. In the soil moisture experiment (AI_SF, "Atmosphere Interactive, Soil Forced") the atmosphere is interactive and soil moisture is prescribed, and vice versa for the nudging experiment (AF_SI, "Atmosphere Forced, Soil Interactive"), where the latter is only used to validate the atmospheric nudging in this study. Finally, in the fully constrained (AF_SF, "Atmosphere Forced, Soil Forced") and soil moisture climatology (AF_SC, "Atmosphere Forced, Soil Climatological") experiments both components are prescribed; once using time-varying and once climatological soil moisture.

70

75   A small ensemble of one or five members is used to create a climatology for each experiment, starting in 1979. The ensembles for AI_SI and AI_SF are enlarged from 5 to 100 members for 2009–2015/2016. As ExtremeX was initiated in 2017 no longer time horizon was proposed. The ensemble size for the other experiments (AF_SI, AF_SC and AF_SF) is constant. CESM has

Earth System
Dynamics
Discussions

Table 1. Overview of experiments and configuration of the model components. The ensemble size for the experiments is given for the two successive simulation periods (# 1979–2008 and # 2009-2015/2016).

Name	Acronym	Atmosphere	Soil Moisture	Ocean	# 1979–2008	# 2009–2015/2016
Control	AI_SI	interactive	interactive	forced	5	100
Soil moisture experiment	AI_SF	interactive	forced	forced	5	100
Nudging experiment	AF_SI	forced	interactive	forced	1 / 5†	1 / 5†
Fully constrained	AF_SF	forced	forced	forced	1 / 5†	1 / 5†
Soil moisture climatology	AF_SC	forced	forced*	forced	1 / 5†	1 / 5†

* Soil moisture is forced using the 1982–2008 climatology of the reconstructed soil moisture time series.

†The modeling groups used different ensemble sizes for the experiments with constrained atmospheric variability. The numbers were constant over the 1979–2015/2016 period for the individual models.

five members for AF_SI and one member for the other experiments with nudged atmosphere. MIROC has five members for all atmosphere nudged experiments and EC-Earth has one. The small ensemble of MIROC and CESM were used to verify that

80   winds at the surface are highly determined by nudging the higher model levels even though in the ExtremeX setup winds are unconstrained in the lowest model levels (Sect. 2.2.1, see also Sect. 4 and Fig. A1). The analysis of the simulations starts in 1982 because the first three simulation years are regarded as spin-up. Likewise, 2009 is regarded as the spin-up for the additional members to diverge and therefore analysis of the years 2010–2015/2016 is recommended for example for event-based analysis of extremes, as is done here.

85   The models were forced with observed or reanalysis data during the observational period and with scenarios thereafter (Sect. 3). The three models choose different scenarios, either the Representative Concentration Pathway 8.5 (RCP8.5; van Vuuren et al., 2011) (CESM), RCP4.5 (MIROC) or the Shared Socio-economic Pathway 3-7.0 (SSP3-7.0; Meinshausen et al., 2020) (EC-Earth). The choice between RCP4.5, RCP8.5 and SSP3-7.0 is not expected to affect the results in this study as the scenarios barely differ for the considered time period.

90

2.2   Methods

The ocean, land surface and atmosphere are constrained to follow observation-based values, either time-varying or climatological ones. All experiments are conducted with SSTs and sea ice concentration prescribed. In the following, the methods to constrain the atmospheric circulation and the land surface are described. We use the terms "forcing" and "constraining"

95   interchangeably for the applied nudging and prescription of the atmospheric winds and/ or soil moisture.

Earth System
Dynamics

Discussions

Open Access

EGU

2.2.1 Constraining of atmospheric circulation

Nudging the atmospheric circulation in a climate model strongly reduces the dynamic variability in a simulation. For ExtremeX, all modeling groups use a grid-point nudging approach (Jeuken et al., 1996) to force the atmospheric large-scale circulation by adding a tendency term to the prognostic equations of the zonal and the meridional wind. This term is computed from the difference between a reference data set and the computed model value. It is weighted by a relaxation time scale (Kooperman et al., 2012), which controls the strength of the constraint. A very short relaxation time scale means a strong constraint of the dynamics while a long relaxation time scale allows larger deviations from the reference. The length of the relaxation time scale is chosen such that it does not dominate model physics but guarantees good agreement with the reference data set. All three models use a 6 h relaxation time scale following Kooperman et al. (2012). The reference data is given by 6-hourly wind fields from the ERA-Interim reanalysis (Dee et al., 2011). At each model time step the nudging term is used to update the horizontal wind variables. Additionally, a height-dependent weighting is introduced which allows a free evolution of the boundary layer while nudging strength increases with height and controls the large-scale circulation (mostly above 700 hPa). The exact implementation of the height-dependent profile was chosen by the groups individually to fit their respective models (Fig. 1).
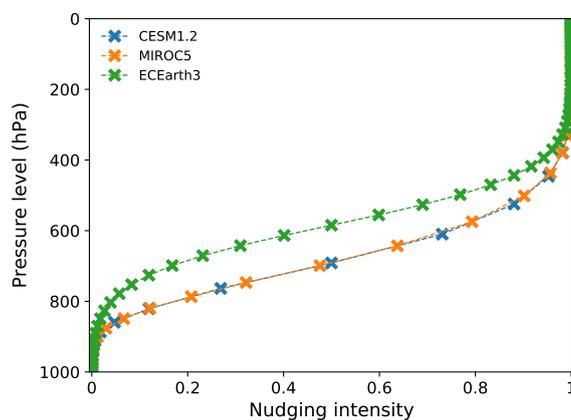
Figure 1. Nudging profile for the three ExtremeX ESMs. The actual pressure levels are marked with an x and joined with lines. The nudging intensity is given from zero (no nudging) to one (fully nudged).

2.2.2 Constraining of soil moisture

Constraining soil moisture in a climate model allows to isolate the main effects of land surface conditions and feedbacks on the climate. In an experiment with an unconstrained atmosphere (AI_SF), the circulation will adapt to the given land surface conditions, but there is no feedback in the opposite direction. Hence, the land is decoupled from the atmosphere. In the present set-up, soil moisture is forced to reflect observed conditions, similar to the SST-driven and nudged-circulation simulations.

115   However, directly prescribing soil moisture from observations or observations-based products (e.g. reanalyses) in a climate
model can lead to inconsistencies due to differences in model climatologies and soil parameterisations (Koster et al., 2009).
Instead, observation-driven soil moisture reconstructions are generated by driving the land surface module of the respective
ESM with observed meteorological observations (e.g. air temperature, humidity, wind, precipitation, radiation). The generated
daily or 6-hourly soil moisture constitutes the model-specific soil moisture reconstruction. This allows soil moisture in the
120   constrained experiments to follow observed soil moisture states, while still being in balance with the model climatologies and
land model parameterisations. The method to constrain the land model with soil moisture reconstructions is inspired by the
approach developed by Hauser et al. (2017) for CESM. Not all models followed the approach in every respect, as it was adapted
to the respective model and tools available (see details in the individual model descriptions in Sect. 3). The common idea is that
the model hydrology is active, but at the end of each time step the modelled soil moisture is replaced with or nudged toward
125   the target soil moisture from the reconstruction.

2.3   Reference data sets

The atmospheric nudging is validated using winds from ERA-Interim (Dee et al., 2011) as reference. Monthly near-surface
temperature is retrieved at $0.5°$ resolution from the Climatic Research Unit, University of East Anglia (Harris et al., 2020),
using version 4.03 of the data set (CRUTS in the following). Precipitation data at $0.5°$ resolution is obtained from the Global
130   Precipitation Climatology Centre full data product version 2018 (GPCC-FD; Ziese et al., 2018). As reference for evapotran-
spiration the LandFlux-Eval data set at $1°$ horizontal resolution is used (Mueller et al., 2013). Total cloud cover information
was retrieved from the International Satellite Cloud Climatology Project D1 (ISCCP-D1; Rossow and Schiffer, 1999) at $2.5°$
resolution. All reference data sets are regridded to the original resolution of each model for the comparison.

2.4   Data analysis

135   In Sect. 5, we disentangle the contribution of the physical drivers (atmospheric circulation, land surface conditions and the
ocean state) and of recent climate change to temperature extremes. The method is briefly explained below, readers can refer
to Wehrli et al. (2019) for more details. The disentangling method only takes anomalies of a variable with respect to the
experiment climatology into account. In this study, the disentangling is applied to anomalies of daily mean temperature and
daily maximum temperature (TX). The different contributions are assumed to be additive and, hence, differences between the
140   experiments are computed. The fully constrained experiment (AF_SF) is taken as the "model truth" because it is as close to
observations as the model can get. Therefore, AF_SF is set to 100 % of the event and the analyses investigate what fraction of
the event anomaly is explained by the other experiments. First, the contribution of recent climate change is computed as the
anomaly of the years 2010–2015/2016 during the same time of the year the event took place (but excluding the event year)
in AI_SI with respect to its 1982–2008 climatology. Note that a small fraction of the 2010–2015/2016 anomalies related to
145   the prescribed SST conditions, could also be due to decadal variability. The anomaly of AI_SI at a specific point in time (e.g.
during an extreme event) compared to its 1982–2008 climatology is a combination of recent climate change (i.e. warming since
the climatology period, which is estimated in the first step using the anomaly of non-event years from AI_SI), the observed

SST pattern, and natural variability. The natural variability is controlled by using a large ensemble of 100 members. Hence, following the additive assumption, the remaining anomaly of AI_SI corresponds to the contribution of the ocean. To estimate

150   the contribution of the land surface state (i.e. soil moisture) and the atmospheric circulation, the disentangling method by Wehrli et al. (2019) follows two approaches. The first approach (A) is to quantify the contribution of soil moisture as the anomaly in AI_SF minus the anomaly in AI_SI and the contribution of the atmospheric circulation as the anomaly in AF_SF minus the anomaly in AI_SF. The second approach (B) is to quantify the contribution of soil moisture as the anomaly of AF_SF minus the anomaly of AF_SC and the contribution of the atmospheric circulation as the anomaly of AF_SC minus the anomaly of

155   AI_SI. Wehrli et al. (2019) show that the two approaches give similar results, which is confirmed here (Sect. 5). Hence, in this study the results from approaches A and B are averaged, giving equal weight to both. The results for the single approaches are also documented in the Appendix. The individual data analysis carried out for four recent heatwaves in Sect. 5.1 and warm spells in Sect. 5.2 is described in the respective sections.

3   Model descriptions

160 ### 3.1   Community Earth System Model (CESM)

The Community Earth System Model is run in Version 1.2 (CESM1.2; Hurrell et al., 2013). Coupled are the Community Atmosphere Model Version 5.3 (CAM5; Neale et al., 2012) and the Community Land Model Version 4 (CLM4; Lawrence et al., 2011; Oleson et al., 2010). Both are run on a horizontal resolution of $0.9° \times 1.25°$. The atmosphere model, CAM5, uses hybrid sigma-pressure coordinates and has 30 vertical layers. CLM4 has 15 soil layers, whereof active hydrology is computed

165   in the upper 10 layers (down to 3.8 m).

    Natural forcings as well as forcings from greenhouse gases (GHGs), aerosols and land-use change follow the setup in Wehrli et al. (2019). Major GHGs (CO_2, N_2O and CH_4) are prescribed to observed global values whereas other anthropogenic forcings follow RCP8.5 after 2005. A merged product of the Hadley Centre sea ice and SST data set Version 1 (HadISST1) and the NOAA weekly optimum interpolation SST analysis Version 2 (OI2) was used to prescribe transient monthly observations of

170   SSTs and sea ice concentrations (Hurrell et al., 2008). For constraining soil moisture the prescription method developed by Hauser et al. (2017) was used, which replaces the model-calculated soil moisture value by a target value at the end of each model time step. The target data set is computed by running CLM4 offline forced by reanalysis data from ERA-Interim. Below $0°C$ soil temperature in the model, soil moisture is computed interactively whereas at warmer temperatures the soil liquid water is prescribed to the total (liquid + ice) soil moisture of the target data set. This prevents artificial creation of ice, which

175   can produce unrealistic heat fluxes (Hauser et al., 2017).

3.2   Model for Interdisciplinary Research on Climate version 5 (MIROC5)

The Model for Interdisciplinary Research on Climate version 5 (MIROC5) was developed jointly at the Atmosphere and Ocean Research Institute, University of Tokyo; National Institute for Environmental Studies; and Japan Agency for Marine-

Earth Science and Technology (Watanabe et al., 2010). The horizontal spectral resolution of the model is T85 (wave number
85 with triangular truncation corresponding to a horizontal resolution of about 160 km). There are 40 vertical model levels
of hybrid sigma-pressure coordinates up to 3 hPa. The land scheme of MIROC5 is an updated version of Minimal Advanced
Treatments of Surface Interaction and Runoff (MATSIRO; Takata et al., 2003), which predicts the temperature and water in
six soil layers down to a depth of 14 m, one canopy layer, and three snow layers. The SST and sea ice concentration data of
HadISST1 were used (Rayner et al., 2003). See Shiogama et al. (2013) for the setup of natural (solar irradiance and volcanic
185 activity) and anthropogenic (GHGs; sulfate, black and organic carbon aerosols; ozone; land use land cover change) forcing
agents. The anthropogenic forcing agents after 2005 were based on RCP4.5.

For constraining soil moisture in MIROC5, the model replaces the calculated soil moisture with a prescribed value at the
beginning of each model time step to force the land state toward the reference. The prescribed soil moisture was simulated
by the land scheme in offline mode using forcing data from ERA-Interim. To remove negative values of liquid soil moisture
190 content, the replacing procedure also limits ice content so that the total soil moisture does not exceed the prescribed one.

3.3 European Community Earth System Model Version 3 (EC-Earth3)

The European Community Earth System Model (EC-Earth3) is a non-operational model with the atmosphere component based
on the European Centre for Medium-Range Weather Forecasts' (ECMWF) Integrated Forecasting System (IFS) and the model
is maintained by the EC-Earth consortium. Version 3.3.1 with IFS cycle cy36r4 was used for the ExtremeX experiments. The
195 horizontal spectral resolution of the model is T255 (about 80 km), and there are 91 vertical model levels. The model has a
hybrid coordinate system combining both sigma coordinates and also reduced Gaussian grid (N128). All experiments were
produced with the SSP3-7.0 CMIP6 scenario and prescribed monthly ocean fields from the merged HadISST1 and NOAA OI2
data set with pre-applied SST/ sea ice consistency checks (Hurrell et al., 2008). More information regarding the model can
be obtained from www.ecmwf.int, www.ec-earth.org, and Döscher et al. (2021, in review) for greenhouse gases, aerosols and
200 land-use prescribed in EC-Earth3.

For constraining soil moisture in EC-Earth, the simulated soil moisture is replaced by the respective target values for each
of the four soil layers at the end of each model time step. As target values, 6-hourly soil moisture data from ERA-Interim/Land
(Balsamo et al., 2015) were used. ERA-Interim/Land uses the H-TESSEL land surface model (Balsamo et al., 2009) which has
four soil layers, covering 0 cm–7 cm, 7 cm–28 cm, 28 cm–100 cm and 100 cm–255 cm of the soil.

205 4 Validation of the constrained atmosphere and soil moisture experiments

Atmospheric nudging forces the simulated horizontal winds toward observations. In the setup used for this study, the nudging
is stronger in the upper atmosphere and close to zero at the surface (Fig. 1). Hence, it can be expected that the variability
between ensemble members is strongly reduced, especially at higher atmospheric levels, and that the simulated winds closely
follow the observations with increasing nudging strength. This is confirmed by evaluating the wind fields of the three models at
210 the grid point level. For MIROC (and less visibly also for CESM; Fig. A1) there is some variability between the five members

of the AF_SI ensemble at near-surface levels, whereas at 500 hPa and above all members are nearly identical and an almost exact representation of the reference. For EC-Earth only one simulation of AF_SI was run. Although the nudging profile of EC-Earth is shifted to higher altitudes compared to the other two models (Fig. 1), the horizontal winds represent the reference equally well. For all models prescribing the large-scale atmospheric flow also has a strong control on near-surface winds.

215   In the following, the climatological model biases are compared between the experiments. First, regional and global RMSEs are examined in Sect. 4.1. Then, the sign and location of seasonal biases is discussed in Sect. 4.2.

4.1   Global and regional biases in surface temperature and precipitation

Intuitively, one might expect that biases with respect to observations are reduced when either soil moisture or atmospheric circulation or both are constrained. Near-surface temperature for example is driven by radiative processes and surface turbulent

220   fluxes. The incoming radiation is related to the abundance, thickness and composition of clouds, which is parameterized in the models and driven by weather systems (e.g. Bony et al., 2015). Surface turbulent fluxes are driven by soil moisture availability, which affects the partitioning in sensible and latent heat fluxes, especially in transitional climate regimes (e.g. Miralles et al., 2019; Santanello et al., 2018; Seneviratne et al., 2010). Similarly, precipitation is affected by both soil moisture and atmospheric circulation. The location and intensity of rainfall and snow is driven by the passage of low and high pressure systems as well

225   as by soil moisture conditions (e.g. van der Ent et al., 2010; Guillod et al., 2015; Moon et al., 2019).

In the following, we quantify the near-surface temperature and precipitation biases in the experiments. Therefore, the model climatologies are compared to a reference by computing the root mean square errors (RMSEs) for the seasonal and annual averages of the 1982–2008 climatology. Only land grid points are considered (except Antarctica).

In the global and annual average, the RMSEs in the experiments with constrained atmosphere and/ or soil moisture are nearly

230   equal to the RMSE in AI_SI (Fig. 2). For EC-Earth the temperature bias increases when soil moisture is prescribed in AI_SF and AF_SF (Fig. 2a). For MIROC a large precipitation bias is introduced when nudging the atmospheric circulation in AF_SI (Fig. 2b). However, the bias is reduced in the fully forced experiment (AF_SF). Temperature biases are largest during the December-January-February (DJF) season in CESM and EC-Earth. In MIROC they are largest during the June-July-August (JJA) season, except for AF_SF where biases are largest in DJF. Precipitation biases are largest in JJA for all models. For

235   the annual regional averages, large temperature biases can be found in regions with sparse observational coverage such as GIC (Greenland/ Iceland), NEN (northeastern North America) and RAR (Russian Arctic; Iturbide et al., 2020, for an overview of the AR6 reference regions see Fig. A2). Large temperature biases can also be found in small regions, which are only represented by a few grid points in the models used, such as NWS (northwestern South America), SWS (southwestern South America) and NZ (New Zealand). Additionally, the complex topography of the Himalayas (TIB) and Andes (SWS and NWS) is also a likely

240   source of temperature biases. Regional precipitation biases are generally larger in wet regions such as the Amazonian regions SAM (South American Monsoon) and NSA (northern South America); and the regions in Central Africa, namely CAF (central Africa), SEAF (southeastern Africa) and NEAF (northeastern Africa); as well as the monsoon regions SEA (southeastern Asia) and SAS (southern Asia). Precipitation biases are also larger for small regions.
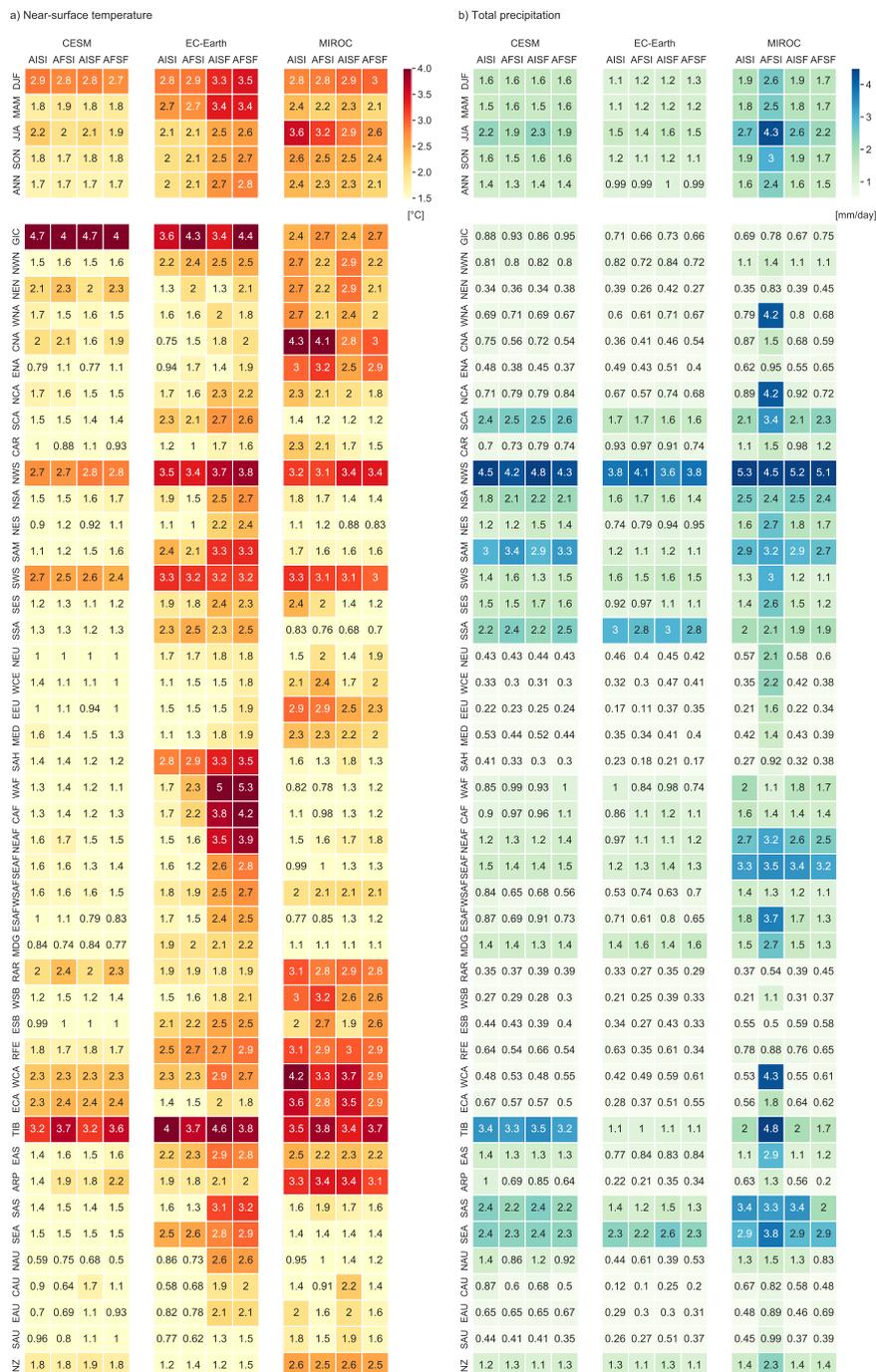
Figure 2. Root mean square errors (RMSEs) for a) near-surface temperature and b) total precipitation. The top section shows the global RMSE for land grid points and seasonal and annual (ANN) averages. The bottom section shows the average annual RMSE for the reference regions from the Sixth Assessment Report (AR6) on climate change (Iturbide et al., 2020). For an overview of the AR6 reference regions see Fig. A2. Ocean grid points and Antarctica are excluded.

In general, the experiments with constrained atmosphere and/ or soil moisture do not show a significant reduction of the
245   surface climatology RMSEs in any of the models or for any region of the world. In many cases constraining the components
of the model leads to even larger biases. This contradicts the initial intuitive assumption and suggests that no sole component
of the model is responsible for the biases and, hence, that these cannot be corrected in isolation.

4.2   Location and sign of seasonal biases

In the Northern Hemisphere mid-latitudes the unconstrained CESM and MIROC models are systematically too hot (Fig. 3a)
250   and in some regions also too dry (Fig. 4a) during boreal summer (JJA). North America, Central Asia and Eastern Europe show
the largest biases. This agrees with the findings by Wehrli et al. (2018) for CESM. For EC-Earth, only Central Asia and parts
of the Midwestern United States are too hot and dry, while other regions are mostly too cold and wet. In all models, the regions
where JJA temperature is overestimated coincide with regions where cloud coverage is underestimated (Fig. A3). Especially
in MIROC, a large negative cloud cover bias can be found for the Northern Hemisphere midlatitudes. In MIROC, large areas
255   in central and eastern North America, eastern Europe and Asia show a negative evapotranspiration bias as well (Fig. A4). In
CESM and EC-Earth evapotranspiration is underestimated in central Asia and parts of western North America. This indicates
that the warm temperature biases are related to underestimated evapotranspiration and cloud coverage in JJA.

Nudging the atmosphere in AF_SI reduces some of the JJA temperature biases in the Northern Hemisphere in CESM and
MIROC (Fig. 3a). For MIROC, large precipitation biases are introduced with nudging (Fig. 4a). Some of the midlatitude
260   regions change from too little precipitation to too much and vice versa. Hence, correcting the atmospheric circulation seems
to lead to an overcompensation of biases in MIROC. In EC-Earth, nudging does not strongly affect the JJA temperature and
precipitation climatology. Constraining the soil moisture in AI_SF leads to a reduction of the hot and dry bias in the Northern
Hemisphere midlatitudes in MIROC. For CESM the changes are smaller but there is a reduction of the hot and dry bias in
Europe and the Midwest. For EC-Earth, constraining the soil moisture, however, introduces or increases the cold and dry bias
265   nearly everywhere. The fully forced experiment (AF_SF) is the experiment with the smallest temperature and precipitation
biases for CESM and MIROC, suggesting that at least for these models a correct representation of atmospheric circulation
patterns and soil moisture conditions can improve the models' performance. Nonetheless, for EC-Earth AF_SF shows larger
biases than AI_SI as the temperature biases introduced in AF_SF outweigh the biases corrected and similarly for precipitation
the biases remain of similar magnitude.

270   The results for the austral summer (DJF) confirm the findings for the Northern Hemisphere in JJA. For EC-Earth, AI_SF
introduces a cold (Fig. 3b) and wet bias (Fig. 4b) in the entire Southern Hemisphere. MIROC shows large precipitation biases
for AF_SI, which are (in certain places) of the opposite sign but similar or larger magnitude than in AI_SI. For CESM there
are only very small differences between the experiments.

All models show substantial biases in total cloud cover fraction (Fig. A3) and evapotranspiration (Fig. A4), which match the
275   biases found in temperature (e.g. negative cloud cover bias and negative evapotranspiration bias for areas that are too warm in
the model) and sometimes also for precipitation. Both variables rely heavily on parameterisations. An alternative explanation
for why biases are still prevalent after correcting the atmospheric flow and the land surface is that ESMs are tuned to match e.g.

11
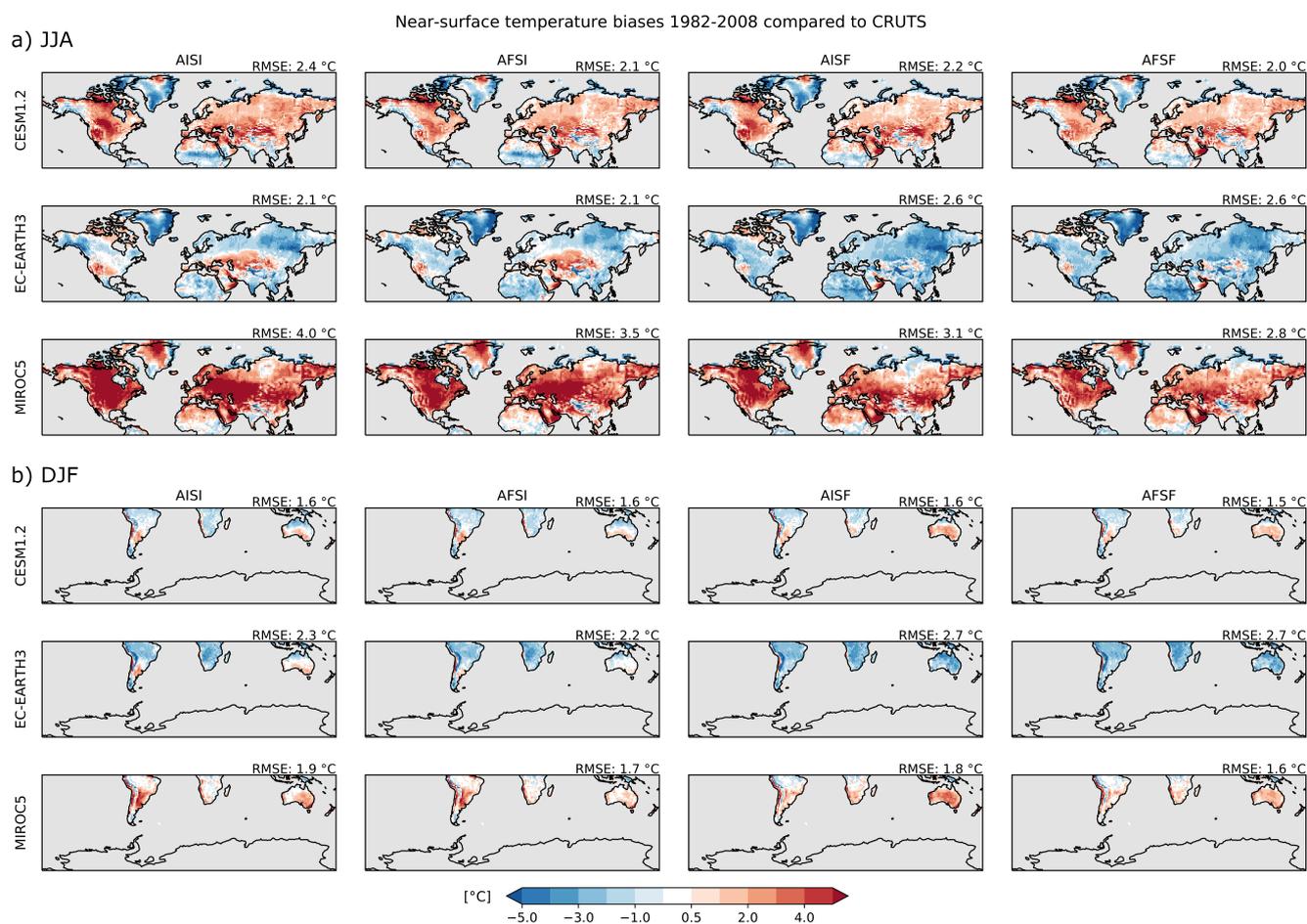
Figure 3. Bias in near-surface temperature (2m) with respect to CRUTS. Shown is the seasonal average over (a) June-July-August (JJA) for the Northern Hemisphere and (b) December-January-February (DJF) for the Southern Hemisphere. The root mean square error (RMSE) averaged over all land grid points of the respective hemisphere is given in the upper right corner of each experiment and model.
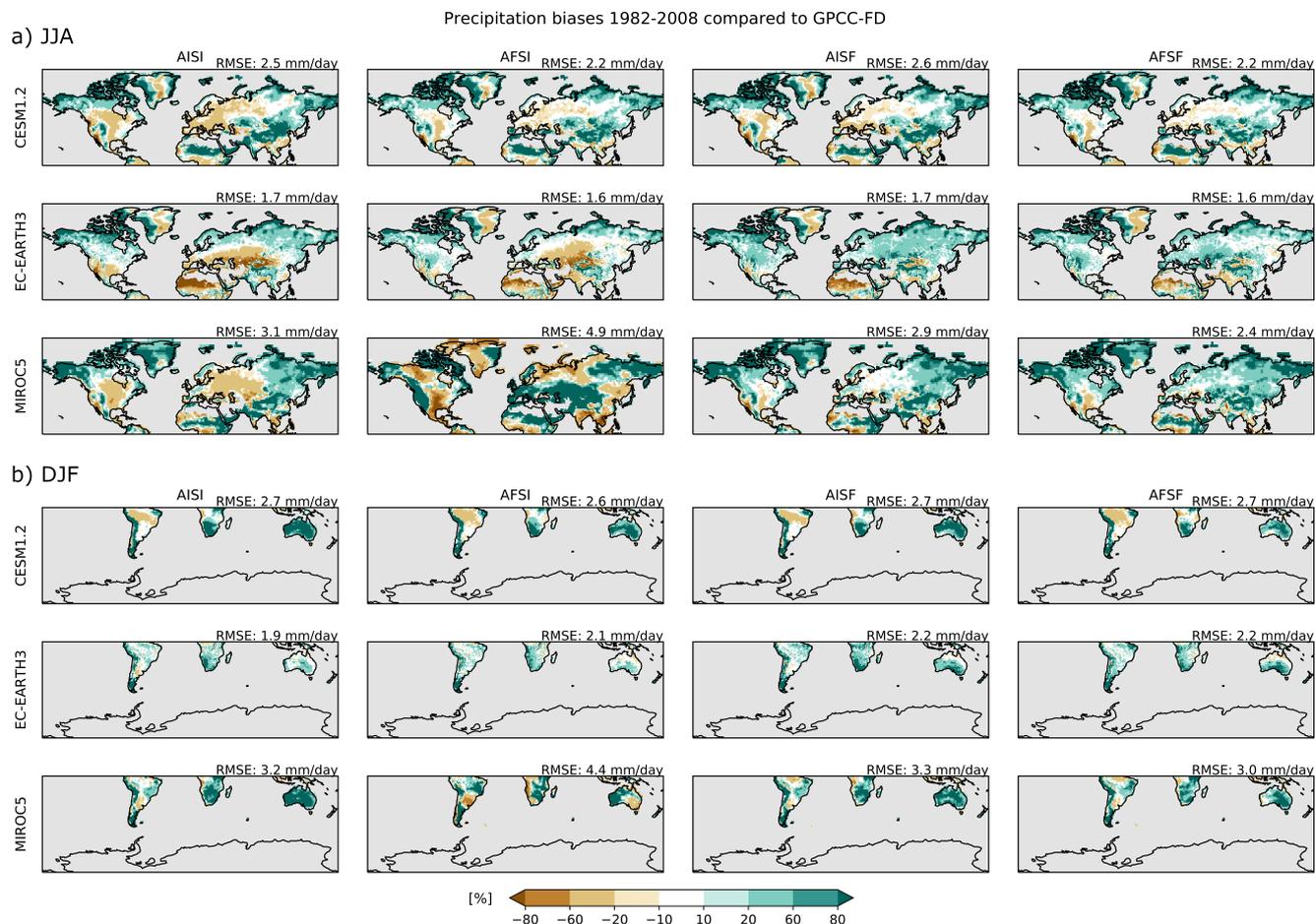
Figure 4. Bias in total precipitation with respect to GPCC-FD. Values are given as percentage deviation from observations. Same as Fig. 3 but RSME given in mm per day.

the radiation balance at the top of the atmosphere and global mean values of variables like near-surface temperature, clouds or sea ice (Mauritsen et al., 2012). When single components of the models are constrained using more realistic fields from observational products, the model components are no longer in balance with each other. This can result in an overcompensation of biases as can be seen for example for precipitation in MIROC (Fig. 4). It is known that MIROC5 shows biases in the North Atlantic storm track activity compared to ERA-Interim (e.g. Zappa et al., 2013). Correcting this circulation bias in AF_SI leads to even larger precipitation biases, which are only reduced when the soil moisture is constrained as well.

Overall, the biases are not substantially reduced in any of the models when constraining the atmospheric circulation or soil moisture using observation-driven reconstructions. This shows that model biases are not primarily caused by the misrepresentation of large-scale atmospheric motion or soil moisture conditions. Instead, the biases might be caused by other processes

such as radiation and cloud processes, convection, precipitation, as well as land surface properties (e.g. land cover and land use, topography). The results also suggest that the models are tuned to have low temperature and precipitation biases in the interactive setup (with prescribed ocean).

290 **5   Disentangling the contribution of physical drivers and climate change to recent heatwaves**

In the previous section it was shown that large biases remain in the model climatology even if observed conditions are used to constrain the models. Nevertheless, nudging the atmospheric large-scale circulation and constraining the soil moisture results in simulations that can accurately reproduce the observed temporal evolution and relative magnitude of events. This was shown by Wehrli et al. (2019) using CESM for five recent heatwaves, considering anomalies of TX. Hence, the presented set

295 of experiments can be used to analyse extreme events if anomalies are used or a more elaborate bias-correction method is performed (e.g. Wehrli et al., 2020). In Sect. 5.1, four recent heatwaves are examined and it is shown that all three models accurately reproduce TX anomalies during and prior to heatwaves, when constrained with observation-based values. Then, the contribution of physical drivers and climate change is disentangled for the four heatwaves. The events chosen are: the 2010 Russian heatwave, the 2015 European heatwave, the 2012 heatwave in the Midwest of the United States, and the Australian

300 heatwave of 2012/2013. All events had drastic consequences to the local communities and the economies due to e.g. damages to agriculture, wildfires and increased mortality. They were investigated in numerous previous studies including Wehrli et al. (2019). The events were chosen due to their severity and impact as well as to ensure consistency and comparability with Wehrli et al. (2019). In Sect. 5.2 warm spells (during the warm season) are analysed grid point-wise to identify the relative contribution of atmospheric circulation vs. soil moisture.

305 **5.1   Driving processes of recent heatwaves**

For four heatwaves the relative contributions of atmospheric circulation, soil moisture, ocean conditions and climate change (since 1982–2008) to TX anomalies are determined. As in Wehrli et al. (2019) spatial averages are taken over the event region and daily mean near-surface temperatures from ERA-Interim are used to identify the events. The hottest 15-day period defines the event and TX during this period is examined. Ocean grid points are excluded from the analysis.

310   TX anomalies (with respect to 1982–2008) for the heatwaves and previous months are shown in Fig. 5. Overall, the fully forced experiments (AF_SF) from all models agree well with observed temperature anomalies and among each other. Small deviations are found during the 2010 Russian heatwave for MIROC, which underestimates the temperature anomaly (Fig. 5a), and during the 2012 Midwest heatwave where CESM overestimates the temperature anomaly (Fig. 5c). In the following, the four heatwaves are analysed separately.

315   For the Russian heatwave of 2010 regional averages are computed over 50°N to 60°N and 35°E to 55°E. The hottest 15-day period lasts from 27 July to 10 August 2010 (Fig. 5a). Observed TX anomalies during the event exceed 10°C, which is captured well by CESM and EC-Earth. In MIROC the anomaly is somewhat weaker. In general, the three models agree on the contributions of the drivers to the TX anomaly (Fig. 6a). They estimate that recent climate change explains around 7%–10%
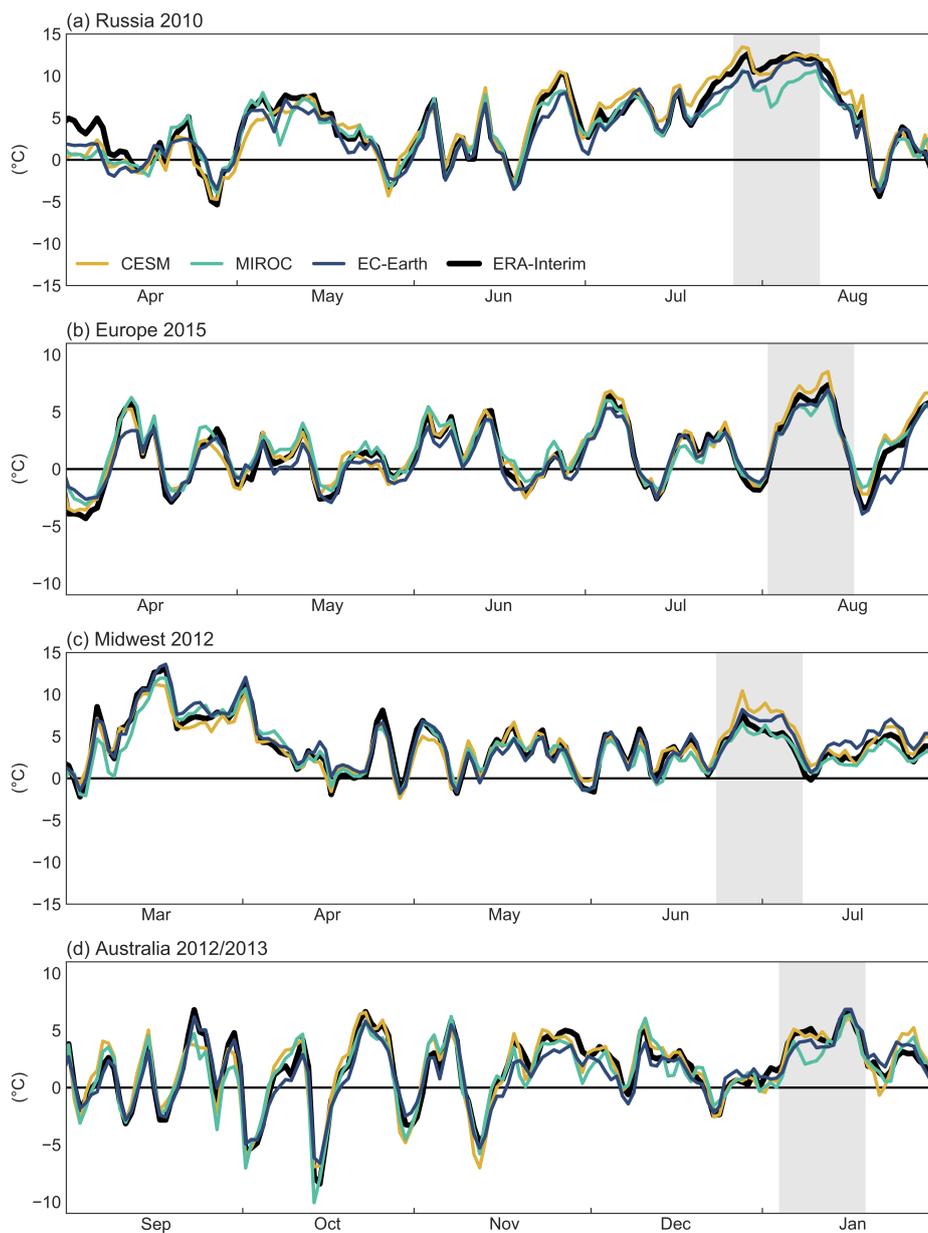
Figure 5. Daily maximum temperature anomaly compared to the 1982–2008 climatology for the fully forced (AF_SF) experiment for the three models and for ERA-Interim (black line). The 15-day event period is highlighted in light grey.
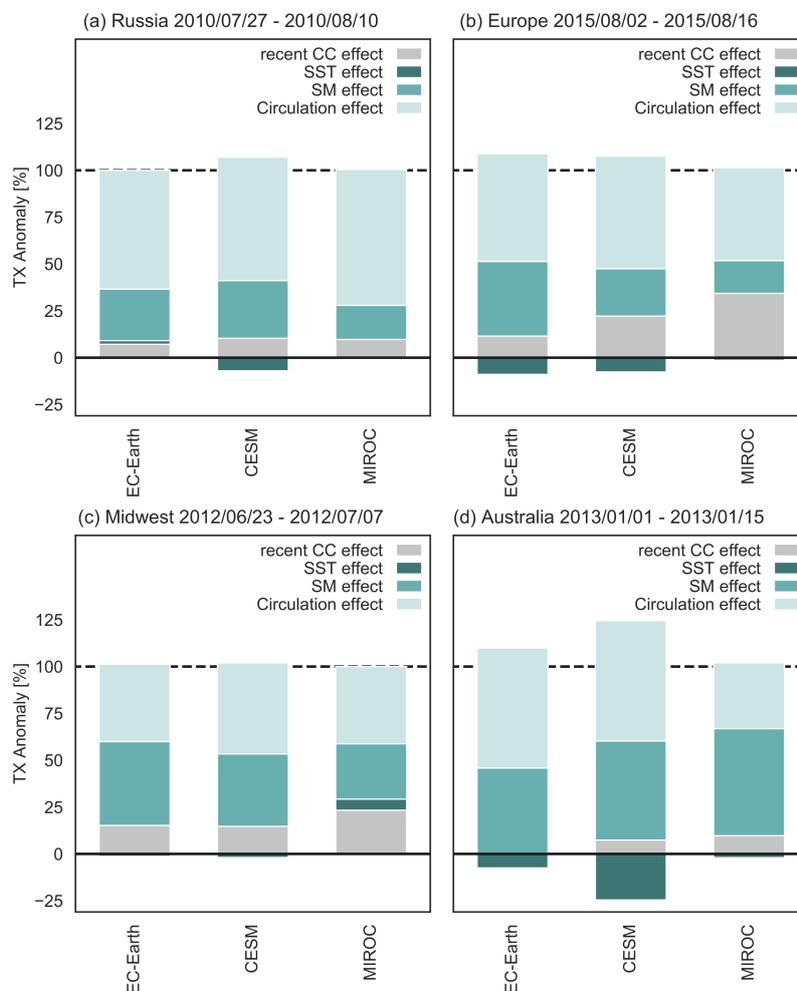
Figure 6. Contribution of recent climate change (since the 1982-2008 base period) and physical drivers to the daily maximum temperature (TX) anomaly during 4 recent events: a) Russia 2010, b) Europe 2015, c) Midwestern U.S. 2012, d) Australian summer 2012/2013. The dates of the hottest consecutive 15-day period are given in the label of each subplot. The contributions of the drivers are normalized by the climatology of AF_SF for each model, respectively. The two approaches to compute SM vs. ATM contribution are merged giving equal weight to both.

of the event anomaly. CESM is the only model which shows a negative ocean contribution of around -7%, whereas the role of

320 the ocean is negligible in the other models. In all three models the event is mostly driven by atmospheric circulation and soil moisture. The ratio of the circulation contribution to the soil moisture contribution is 70:30 for EC-Earth and CESM and 80:20 for MIROC. Assessing the two approaches to disentangle atmospheric circulation from soil moisture contributions separately gives very similar results (Fig. A5a).

The European heatwave of 2015 is analysed over the Western and Central Europe (WCE) AR6 reference region (Iturbide et al., 2020, same as Central Europe (CEU) from previous assessment reports). The hottest 15-day period is from 2 August to 16 August 2015 (Fig. 5b). The magnitude of the TX anomaly before and during the heatwave is represented well by all models. However, there are differences in the attribution of the drivers. In EC-Earth, climate change contributes around 12% to the event anomaly, whereas in CESM climate change is estimated to contribute 22% and in MIROC 34% (Fig. 6b). EC-Earth and CESM agree that there is a small negative contribution by the ocean of -9% and -7%, respectively. In MIROC the ocean is negligible for the event anomaly (around -1%). The three models agree on the magnitude of the atmospheric circulation contribution, which is around half of the total event anomaly. However, the role of soil moisture depends on how much of the event anomaly is attributed to recent climate change. EC-Earth estimates the highest relative soil moisture contribution with a ratio of 60:40 between circulation and soil moisture. The ratio is 70:30 for CESM and 75:25 for MIROC. The results for the two disentangling approaches differ most notably for EC-Earth, where the ratios are nearly balanced for one approach (B) and 65:35 for the other (A; Fig A5b).

For the Midwest heatwave of 2012 the region from 35°N to 50°N and 55°W to 110°W is assessed. The event is analysed from 23 June to 7 July (Fig. 5c). The TX anomaly is represented well by MIROC and EC-Earth and a bit overestimated in CESM. The models agree well on the relative contribution of the drivers. In EC-Earth and CESM, recent climate change explains around 15% of the event anomaly, whereas for MIROC it is slightly more (23%, Fig. 6c). All models agree that the role of the ocean is very small, even if the sign is negative for EC-Earth and CESM (both -1%) but positive for MIROC (6%). The three models agree that the role of soil moisture conditions is about equal to the role of atmospheric circulation. The ratio of circulation to soil moisture contribution is 50:50 for EC-Earth, 55:45 for CESM and 60:40 for MIROC. The individual results for the disentangling approaches show that for all models soil moisture dominates for one approach (A) while atmospheric circulation dominates for the other (B) (Fig. A5c).

The Australian heatwave of 2012/2013 is analysed for the region from 18°S to 30°S and 133°E to 147°E. The hottest consecutive 15-days occur just at the beginning of 2013 from 1 January to 15 January 2013 (Fig. 5d). The models represent the observed TX anomaly mostly well, except that in MIROC it is underestimated during the first half of the event period. While the contribution by recent climate change to the event anomaly is very small and negative in EC-Earth (-2%), CESM and MIROC agree on a small but positive contribution (7% and 10%, respectively, Fig. 6d). All models show a negative contribution of the ocean, which is most notable in CESM (around -25%), while in EC-Earth it is smaller (-7%) and almost negligible in MIROC (-2%). For EC-Earth and CESM the contribution by the atmospheric circulation is larger than by soil moisture, whereas for MIROC it is the other way around. The ratio of atmospheric circulation contribution to soil moisture contribution is 60:40 for EC-Earth, 55:45 for CESM and 40:60 for MIROC. For MIROC, the individual ratios from the two disentangling approaches are similar and both agree that the contribution of soil moisture is larger than the contribution of the atmospheric circulation to the event anomaly (Fig. A5d).

Overall, the three models agree well on the relative contribution of atmospheric circulation vs. soil moisture to the TX anomaly during four recent heatwaves. For the heatwaves of 2010 in Russia and 2015 in Europe, all models show that the atmospheric circulation plays the most important role. For the Midwest heatwave 2012 the models agree, that soil moisture

conditions are about as important as atmospheric circulation for driving the TX anomaly. For the Australian heatwave of
2012/2013 two models show that atmospheric circulation is more important whereas one model shows that the soil moisture
contribution was largest. All models agree on a small role of climate change in driving the TX anomaly during the 2010 Russian
heatwave and the 2012/2013 heatwave in Australia. However, for the 2015 European heatwave and the Midwestern heatwave
in 2012 the role of climate change differs between the models, being largest for MIROC and smallest for EC-Earth. The role of
the ocean is small for the heatwaves of 2010 in Russia, 2015 in Europe and 2012 in the Midwest. For the 2012/2013 heatwave
in Australia all models agree that the role of the ocean is negative – thus not favoring a heatwave – however, the models disagree
on the magnitude, with CESM being the only model displaying a notable contribution by the ocean.

5.2 Relative contribution of atmospheric circulation and soil moisture to episodes of anomalously warm temperatures

In the following, we analyse the role of atmospheric circulation and soil moisture in driving the occurrence of warm spells
during 1982–2015/2016 (2015 for MIROC and 2016 for the other two models). The disentangling method is the same as used
previously in Sect. 5.1. Warm spells are defined grid point-wise as time periods during the local summer season where daily
mean temperature anomalies in ERA-Interim exceed 1.5 standard deviations of the 1982–2010 climatology for at least three
consecutive days. A 7-day running mean is applied to the years 1982–2010 from ERA-Interim before computing the daily
climatology and standard deviation. The local summer season is defined as the three hottest consecutive months. The threshold
of 1.5 standard deviations was chosen such that most regions of the world actually experience events. However, using 1 or
2 standard deviations as threshold leads to very similar results (not shown). The identified warm spells are categorised into
events of 3–5 days, 6–13 days and 14 days and longer. The spells are analysed by taking the same dates in the experiments.
One or five ensemble members (over the years 1982–2015/2016) are used, depending on how many were available per model
and experiment. The mean temperature anomaly of each event category and experiment is used to disentangle the relative
contribution of the atmospheric circulation and soil moisture conditions grid point-wise. The agreement among models is very
high for all spell lengths (Fig. 7). The grid points where soil moisture contributes one third or more to the warm spells, agree
well with the regions of high soil moisture-temperature coupling (Koster et al., 2004; Miralles et al., 2012). With increasing
spell length, the contribution of soil moisture becomes more important, for example in the U.S. Midwest, Eurasia and northern
Australia.

The analysis also reveals that warm spells of 14 days and longer with a magnitude of more than 1.5 standard deviation do
not occur often or in many regions of the world. The result for eastern Europe, for example, can be traced back to the Russian
heatwave in 2010. For regions that see perennial ice and permafrost, like Greenland or Siberia, it is not always possible to
disentangle the relative contributions of atmosphere and soil moisture. But also for Amazonia the contributions cannot be
disentangled. This is because differences are computed that can become negative if the less constrained experiments have a
higher temperature anomaly than the more constrained experiments on average. The affected grid cells are masked out in grey
together with ocean grid points in Fig. 7.

It has to be noted, that the analysis method takes into account the temporal persistence of warm spells but not temporal
correlation as for example the time-lagged effect of dry springs on hot summers (e.g. Hirschi et al., 2011; Quesada et al.,
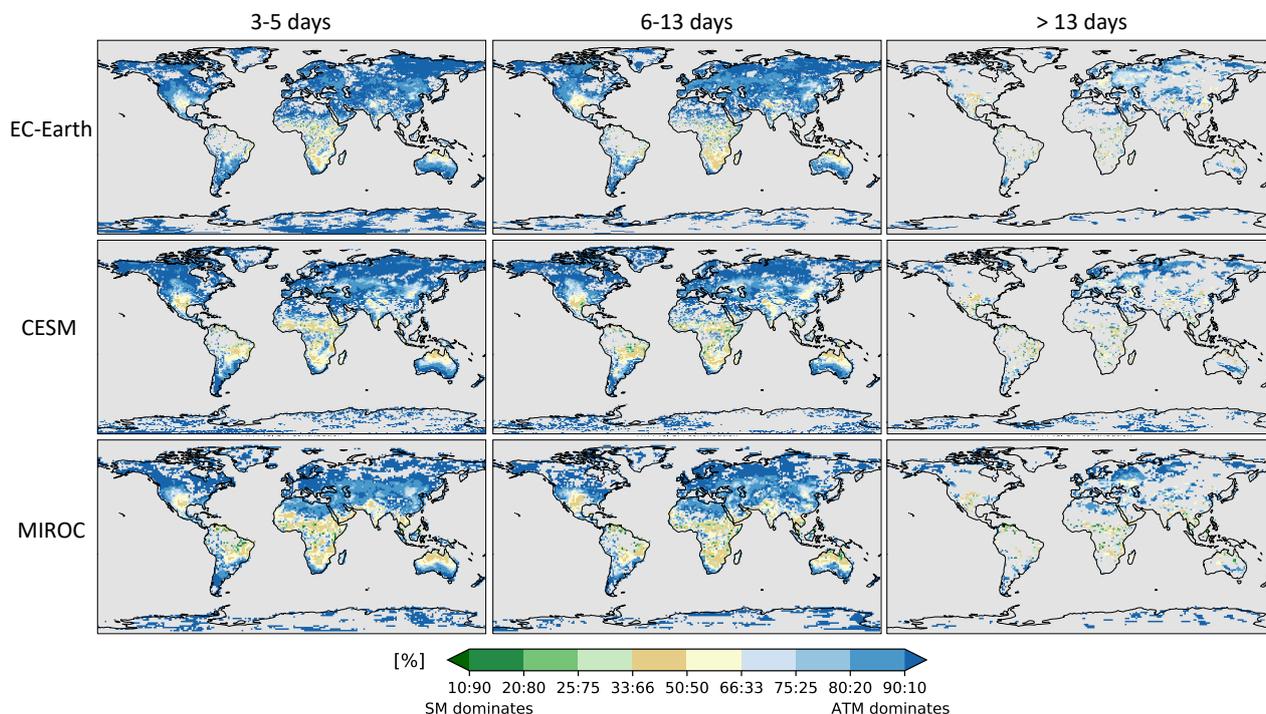
Figure 7. Contribution of atmospheric circulation (ATM) vs. soil moisture (SM) to warm spells where daily mean temperature anomalies exceed 1.5 standard deviation from the ERA-Interim 1981–2010 climatology. The two approaches to compute SM vs. ATM contribution are merged giving equal weight to both. Events are categorised into spells lasting 3–5 days, 6–13 days and 14 days and longer. Grid points where no events where identified or the contributions could not be determined (see text) are masked out in grey together with ocean grid points.

2012). Furthermore, the events are only identified grid-point wise and not as spatially coherent patterns, as they would occur naturally. This is responsible for some of the noise in the patterns.

6 Conclusions and outlook

The ExtremeX experiment is a multi-model intercomparison project designed to study processes contributing to the occurrence and intensity of extreme events. ExtremeX currently consists of simulations with three ESMs: EC-Earth3, MIROC5 and CESM1.2. Five experiments with varying levels of forcing were run with all models. A grid-point nudging approach is used to constrain the modeled horizontal winds in the atmosphere and soil moisture nudging or prescription is used to constrain the land surface.

Although the constrained experiments allow to capture well the temporal evolution and magnitude of temperature anomalies during recent heatwave events, climatological biases in temperature and precipitation remain in the experiments. This is the case both for experiments with either observationally-constrained atmospheric circulation patterns and/ or soil moisture conditions.

In some cases, even larger biases appear in the constrained experiments (Fig. 2). Comparing the location and magnitude of

405   the climatological biases reveals that the patterns and sign of the biases often remain and the magnitude is only marginally

reduced. This agrees with findings by Wehrli et al. (2018) for atmospheric nudging in CESM. The results suggest that the

biases are caused by other processes such as cloud and precipitation formation, convection and interactions of the land surface

and the ocean with the atmosphere, or also land surface parameters. It is also likely that none of these other elements is the sole

explanation for the climatological biases, but rather their interaction, including with atmospheric circulation and soil moisture

410   dynamics.

Despite the biases in mean climatology, the experiments with constrained atmosphere and soil moisture can accurately

reproduce observed temperature anomalies during and prior to heatwaves (Fig. 5). This is found for all models and supports

the results by Wehrli et al. (2019) for CESM. Thus, the presented set of experiments can be used for extreme event analysis

as long as the atmospheric circulation and/ or soil moisture are major drivers of the event. The result also implies that bias

415   correction could be used to improve the representation of observed extreme events instead of analysing anomalies. The present

study disentangles the role of atmospheric circulation vs. land surface processes for temperature anomalies. Following the

disentangling in Wehrli et al. (2019), experiments with constrained soil moisture (AI_SF) and with nudged atmosphere and

soil moisture constrained to climatological values (AF_SC) are used along with the control (AI_SI) and fully constrained

(AF_SF) experiments. Because atmospheric nudging also strongly constrains land-atmosphere interactions the experiment

420   with nudged atmosphere and interactive soil moisture (AF_SI) is not considered. However, strong soil moisture anomalies

might also influence the circulation in some cases (e.g. Teng et al., 2019). In general, this effect is minor compared to the land

reacting to atmospheric conditions and furthermore, two disentangling approaches are considered as in Wehrli et al. (2019) to

have more robust results. Nevertheless, it has to be noted that disentangling causality in a coupled system always comes with

limitations.

425   TX anomalies during four recent heatwaves are attributed to their physical drivers and to climate change. The four events

considered are: the 2010 Russian heatwave, the 2012 heatwave in the Midwest of the United States, the Australian heatwave

of 2012/2013 and the European heatwave in 2015. Overall the models show good agreement on the role of the drivers. Recent

warming (since 1982–2008) is found to positively contribute to the event anomaly for all events and nearly all models (not for

the Australian heatwave 2012/2013 and EC-Earth). The largest contribution is found for the Midwest heatwave 2012 (15%–

430   23%) and for the European heatwave 2015, however for the latter event the three models agree less on the relative role of

climate change (12%–34%). The ocean was not found to have a substantial role in driving any of the events considered. For the

Australian heatwave 2012/2013 the ocean is found to influence the temperature anomaly negatively in CESM (-23%). This is

in accordance with the cool to neutral phase of the El Niño Southern Oscillation (NOAA Climate Prediction Center, 2021). For

all four heatwaves the models show that both atmospheric circulation and land surface conditions significantly contribute to the

435   event anomaly. For the Russian heatwave 2010 and the European heatwave 2015 atmospheric circulation is the dominant driver

with land surface conditions playing a secondary but still important role. Yet, for the Midwest heatwave 2012, soil moisture is

about as important as atmospheric circulation and for the Australian heatwave 2012/2013 one model shows that soil moisture

is the most important driving factor and the other two models show that the two physical drivers are about equally important.

The experiments also allow a general assessment of the respective contributions of circulation anomalies vs. soil moisture
440   conditions for warm spells. The results are very similar for the three ESMs showing that the models generally agree on the
representation of extreme events and the driving processes behind these events. Warm spells of at least 3 days length are
assessed grid point-wise and show that soil moisture is responsible for around one third to half of the temperature anomalies in
transitional and tropical climate zones (Fig. 7). The regions identified resemble the regions of strong soil moisture-temperature
coupling highlighted by Miralles et al. (2012) for observational data and Seneviratne et al. (2006) for global climate models.
445   Both studies additionally identify southern Europe and Eurasia as regions of strong soil moisture-temperature coupling which
is, however, not confirmed from the results presented here. Nevertheless, in regions where spells of at least two weeks can
occur – like in Eurasia – soil moisture is more important than for shorter events, driving up to one third of the temperature
anomaly.

This study expands the mechanistic analysis of recent heatwaves by Wehrli et al. (2019) using three Earth System Models.
450   The results at the grid point level and for the four heatwaves suggest that both circulation patterns and soil moisture anomalies
substantially contribute to the occurrence of heat extremes, consistent with Wehrli et al. (2019). Soil moisture effects are
particularly important in the tropics, monsoon regions, and the US Great Plains, while circulation anomalies tend to dominate
in other regions of the extratropics. These results can help to shed light on processes that need to be better taken into account in
weather predictions and climate projections. For instance, the important role of soil moisture conditions for extremes suggests
455   that soil moisture monitoring and initialization could substantially help improve weather prediction of extremes in several
regions.

Code and data availability.   The code and data can be made available by the authors upon request.

Earth System
Dynamics
Discussions

Open Access

EGU

Figure A1. Comparison of winds for the experiments with nudged atmosphere (NDG, corresponds to AF_SI) and free atmosphere (CTL, corresponds to AI_SI). Shown are 6-hourly wind direction (a) and wind speed (b) during one month (June 2000) for one grid point over the Alps. The winds from the models were interpolated to 250 hPa, 500 hPa and 850 hPa. The winds from ERA-Interim (ERAI target) were interpolated to the same pressure levels and the model resolution for each model.

AR6 reference regions
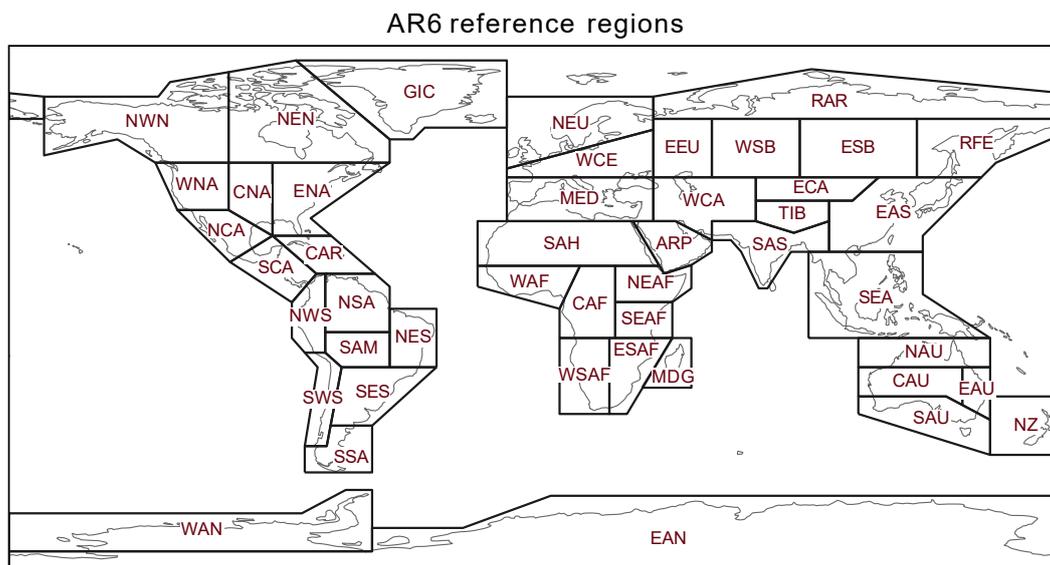
Abbrev.	Name	Abbrev.	Name	Abbrev.	Name
GIC	Greenland/Iceland	NEU	N.Europe	RFE	Russian-Far-East
NWN	N.W.North-America	WCE	West&Central-Europe	WCA	W.C.Asia
NEN	N.E.North-America	EEU	E.Europe	ECA	E.C.Asia
WNA	W.North-America	MED	Mediterranean	TIB	Tibetan-Plateau
CNA	C.North-America	SAH	Sahara	EAS	E.Asia
ENA	E.North-America	WAF	Western-Africa	ARP	Arabian-Peninsula
NCA	N.Central-America	CAF	Central-Africa	SAS	S.Asia
SCA	S.Central-America	NEAF	N.Eastern-Africa	SEA	S.E.Asia
CAR	Caribbean	SEAF	S.Eastern-Africa	NAU	N.Australia
NWS	N.W.South-America	WSAF	W.Southern-Africa	CAU	C.Australia
NSA	N.South-America	ESAF	E.Southern-Africa	EAU	E.Australia
NES	N.E.South-America	MDG	Madagascar	SAU	S.Australia
SAM	South-American-Monsoon	RAR	Russian-Arctic	NZ	New-Zealand
SWS	S.W.South-America	WSB	W.Siberia	EAN	E.Antarctica
SES	S.E.South-America	ESB	E.Siberia	WAN	W.Antarctica
SSA	S.South-America				

Figure A2. Reference regions of the IPCC AR6 as defined in Iturbide et al. (2020).
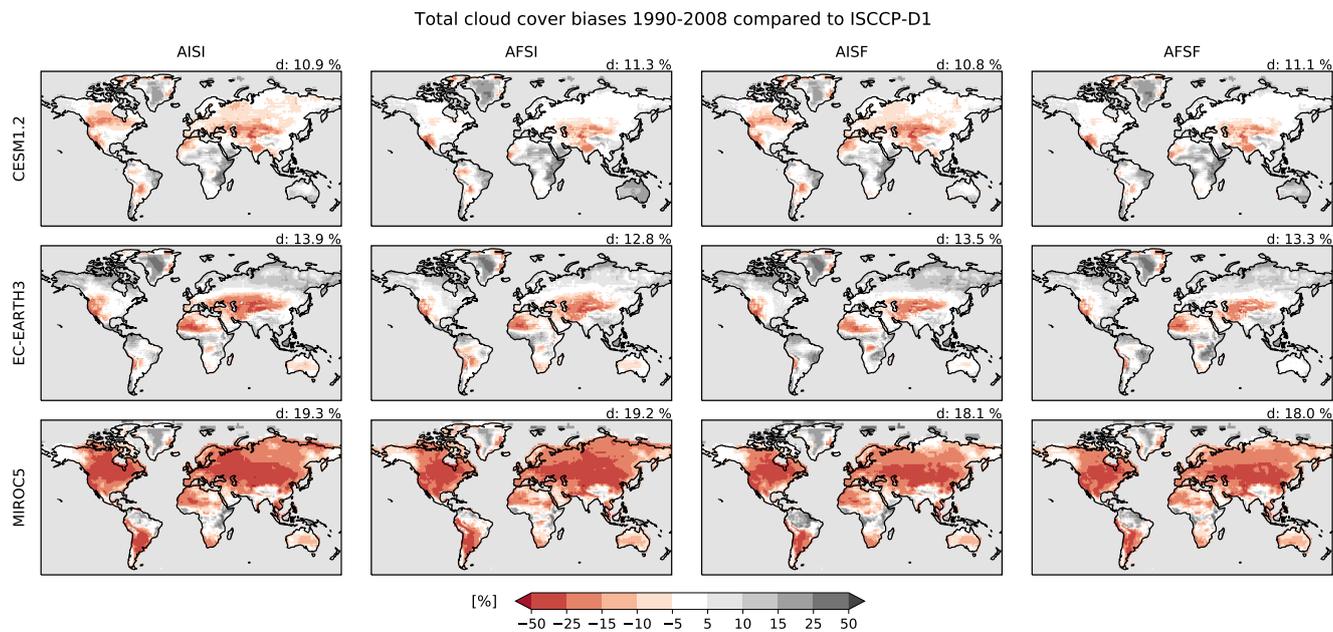
Figure A3. Bias in total cloud cover with respect to ISCCP-D1. Average for the June-July-August season.
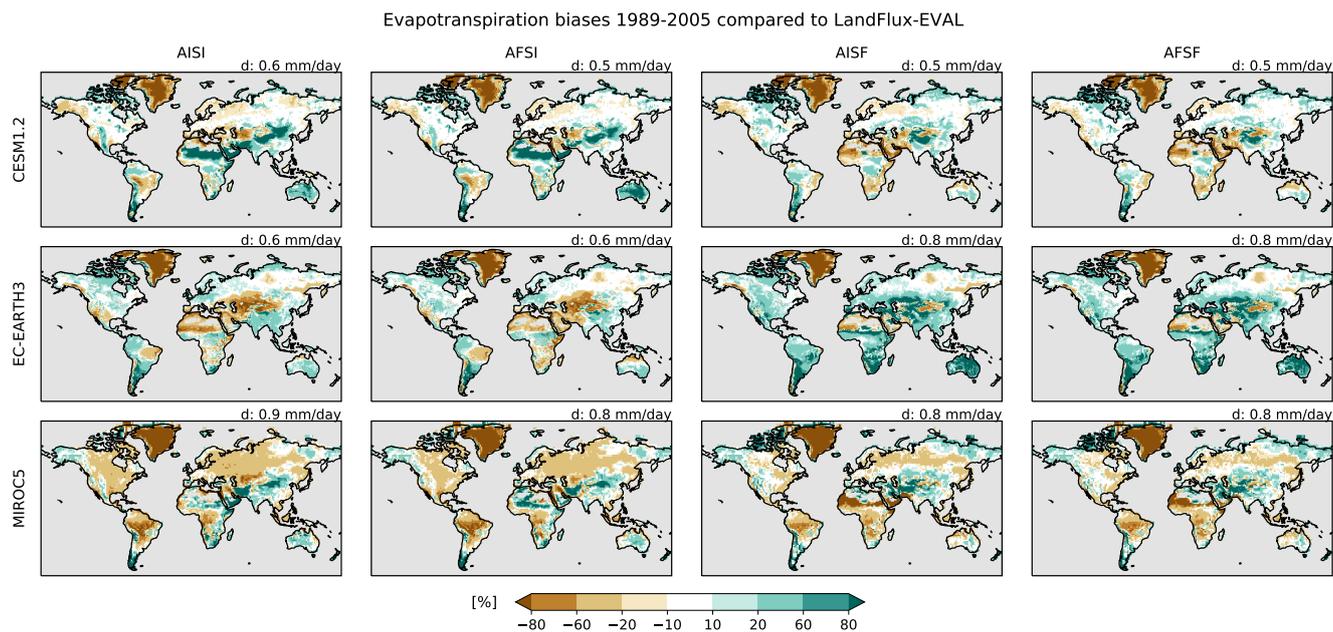
Figure A4. Bias in evapotranspiration with respect to LandFlux-Eval. Average for the June-July-August season.

Earth System
Dynamics
Discussions
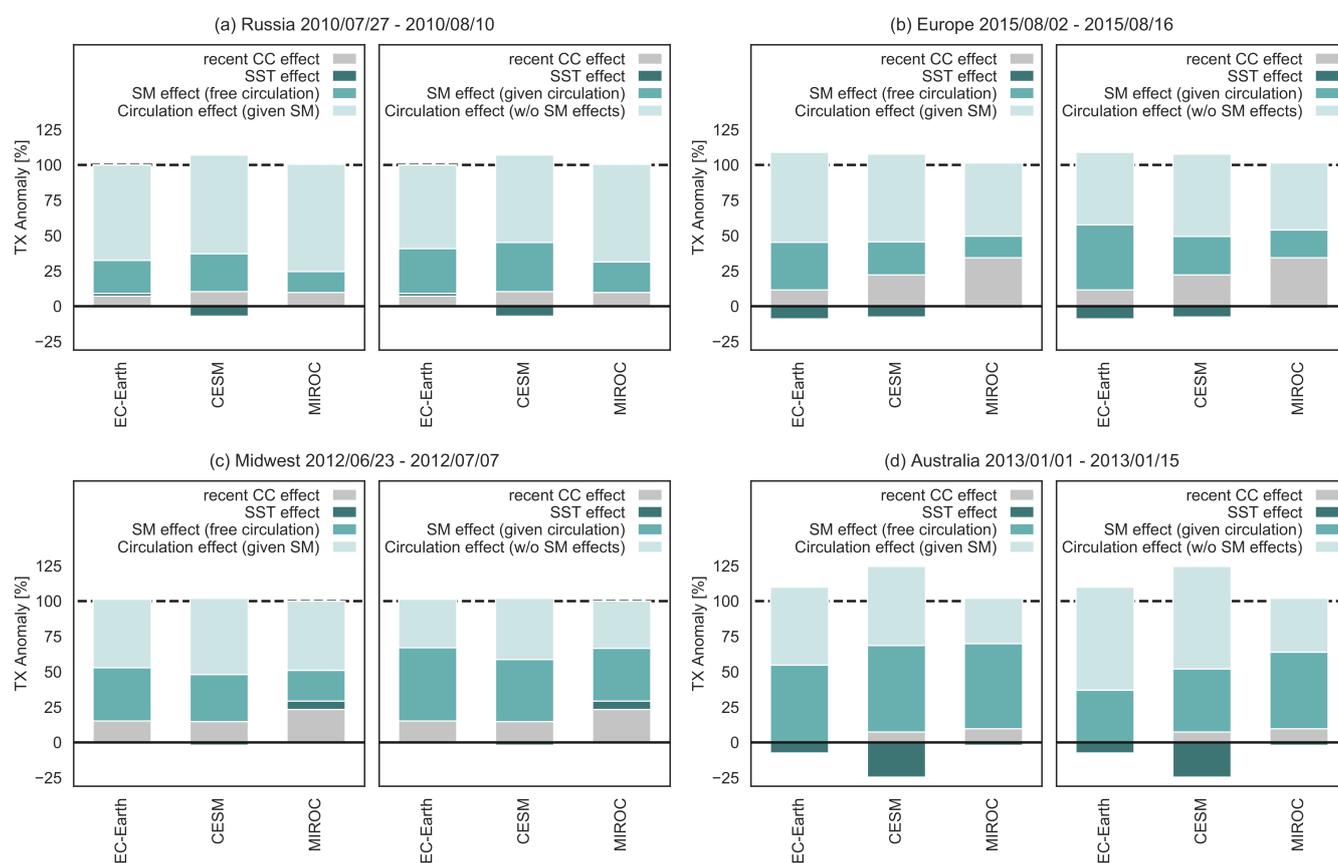
Figure A5. Same as Fig. 6 but showing the separate effects for the two approaches to compute SM vs. ATM contributions (left A, right B).

References

Angélil, O., Perkins-Kirkpatrick, S., Alexander, L. V., Stone, D., Donat, M. G., Wehner, M., Shiogama, H., Ciavarella, A., and Christidis, N.:

475   Comparing regional precipitation and temperature extremes in climate model and reanalysis products, Weather and Climate Extremes, 13, 35–43, https://doi.org/10.1016/j.wace.2016.07.001, 2016.

Balsamo, G., Beljaars, A., Scipal, K., Viterbo, P., van den Hurk, B., Hirschi, M., and Betts, A. K.: A revised hydrology for the ECMWF model: verification from field site to terrestrial water storage and impact in the integrated forecast system, Journal of Hydrometeorology, 10, 623–643, https://doi.org/10.1175/2008JHM1068.1, 2009.

480   Balsamo, G., Albergel, C., Beljaars, A., Boussetta, S., Brun, E., Cloke, H., Dee, D., Dutra, E., Muñoz Sabater, J., Pappenberger, F., de Rosnay, P., Stockdale, T., and Vitart, F.: ERA-Interim/Land: a global land surface reanalysis data set, Hydrology and Earth System Sciences, 19, 389–407, https://doi.org/10.5194/hess-19-389-2015, 2015.

Bony, S., Stevens, B., Frierson, D. M. W., Jakob, C., Kageyama, M., Pincus, R., Shepherd, T. G., Sherwood, S. C., Siebesma, A. P., Sobel, A. H., Watanabe, M., and Webb, M. J.: Clouds, circulation and climate sensitivity, Nature Geoscience, 8, 261–268,

485   https://doi.org/10.1038/ngeo2398, 2015.

Dee, D. P., Uppala, S. M., Simmons, A. J., Berrisford, P., Poli, P., Kobayashi, S., Andrae, U., Balmaseda, M. A., Balsamo, G., Bauer, P., Bechtold, P., Beljaars, A. C. M., van de Berg, L., Bidlot, J., Bormann, N., Delsol, C., Dragani, R., Fuentes, M., Geer, A. J., Haim-berger, L., Healy, S. B., Hersbach, H., Hólm, E. V., Isaksen, L., Kållberg, P., Köhler, M., Matricardi, M., McNally, A. P., Monge-Sanz, B. M., Morcrette, J.-J., Park, B.-K., Peubey, C., de Rosnay, P., Tavolato, C., Thépaut, J.-N., and Vitart, F.: The ERA-Interim reanalysis:

490   configuration and performance of the data assimilation system, Quarterly Journal of the Royal Meteorological Society, 137, 553–597, https://doi.org/10.1002/qj.828, 2011.

Döscher, R., Acosta, M., Alessandri, A., Anthoni, P., Arneth, A., Arsouze, T., Bergmann, T., Bernadello, R., Bousetta, S., Caron, L.-P., Carver, G., Castrillo, M., Catalano, F., Cvijanovic, I., Davini, P., Dekker, E., Doblas-Reyes, F. J., Docquier, D., Echevarria, P., Fladrich, U., Fuentes-Franco, R., Gröger, M., v. Hardenberg, J., Hieronymus, J., Karami, M. P., Keskinen, J.-P., Koenigk, T., Makkonen, R., Massonnet,

495   F., Ménégoz, M., Miller, P. A., Moreno-Chamarro, E., Nieradzik, L., van Noije, T., Nolan, P., O'Donnell, D., Ollinaho, P., van den Oord, G., Ortega, P., Prims, O. T., Ramos, A., Reerink, T., Rousset, C., Ruprich-Robert, Y., Le Sager, P., Schmith, T., Schrödner, R., Serva, F., Sicardi, V., Sloth Madsen, M., Smith, B., Tian, T., Tourigny, E., Uotila, P., Vancoppenolle, M., Wang, S., Wårlind, D., Willén, U., Wyser, K., Yang, S., Yepes-Arbós, X., and Zhang, Q.: The EC-Earth3 Earth System Model for the Climate Model Intercomparison Project 6, Geoscientific Model Development Discussions, pp. 1–90, https://doi.org/10.5194/gmd-2020-446, 2021.

500   Flato, G., Marotzke, J., Abiodun, B., Braconnot, P., Chou, S., Collins, W., Cox, P., Driouech, F., Emori, S., Eyring, V., Forest, C., Gleckler, P., Guilyardi, E., Jakob, C., Kattsov, V., Reason, C., and Rummukainen, M.: Evaluation of climate models, book section 9, pp. 741–866, Cambridge University Press, Cambridge, United Kingdom and New York, NY, USA, https://doi.org/10.1017/CBO9781107415324.020, 2013.

Guillod, B. P., Orlowsky, B., Miralles, D. G., Teuling, A. J., and Seneviratne, S. I.: Reconciling spatial and temporal soil moisture effects on

505   afternoon rainfall, Nature Communications, 6, https://doi.org/10.1038/ncomms7443, 2015.

Harris, I., Osborn, T. J., Jones, P., and Lister, D.: Version 4 of the CRU TS monthly high-resolution gridded multivariate climate dataset, Scientific Data, 7, https://doi.org/10.1038/s41597-020-0453-3, 2020.

Hauser, M., Orth, R., and Seneviratne, S. I.: Investigating soil moisture–climate interactions with prescribed soil moisture experiments: An assessment with the Community Earth System Model (version 1.2), Geoscientific Model Development, 10, 1665–1677, https://doi.org/10.5194/gmd-10-1665-2017, 2017.

Hirschi, M., Seneviratne, S. I., Alexandrov, V., Boberg, F., Boroneant, C., Christensen, O. B., Formayer, H., Orlowsky, B., and Stepanek, P.: Observational evidence for soil-moisture impact on hot extremes in southeastern Europe, Nature Geosci, 4, 17–21, https://doi.org/10.1038/ngeo1032, 2011.

Hurrell, J. W., Hack, J. J., Shea, D., Caron, J. M., and Rosinski, J.: A new sea surface temperature and sea ice boundary dataset for the Community Atmosphere Model, Journal of Climate, 21, 5145–5153, https://doi.org/10.1175/2008JCLI2292.1, 2008.

Hurrell, J. W., Holland, M. M., Gent, P. R., Ghan, S., Kay, J. E., Kushner, P. J., Lamarque, J.-F., Large, W. G., Lawrence, D., Lindsay, K., Lipscomb, W. H., Long, M. C., Mahowald, N., Marsh, D. R., Neale, R. B., Rasch, P., Vavrus, S., Vertenstein, M., Bader, D., Collins, W. D., Hack, J. J., Kiehl, J., and Marshall, S.: The Community Earth System Model: a framework for collaborative research, Bulletin of the American Meteorological Society, 94, 1339–1360, https://doi.org/10.1175/BAMS-D-12-00121.1, 2013.

Iturbide, M., Gutiérrez, J. M., Alves, L. M., Bedia, J., Cerezo-Mota, R., Cimadevilla, E., Cofiño, A. S., Di Luca, A., Faria, S. H., Gorodetskaya, I. V., Hauser, M., Herrera, S., Hennessy, K., Hewitt, H. T., Jones, R. G., Krakovska, S., Manzanas, R., Martínez-Castro, D., Narisma, G. T., Nurhati, I. S., Pinto, I., Seneviratne, S. I., van den Hurk, B., and Vera, C. S.: An update of IPCC climate reference regions for subcontinental analysis of climate model data: Definition and aggregated datasets, Earth System Science Data, 12, 2959–2970, https://doi.org/10.5194/essd-12-2959-2020, 2020.

Jeuken, A. B. M., Siegmund, P. C., Heijboer, L. C., Feichter, J., and Bengtsson, L.: On the potential of assimilating meteorological analyses in a global climate model for the purpose of model validation, Journal of Geophysical Research: Atmospheres, 101, 16 939–16 950, https://doi.org/10.1029/96JD01218, 1996.

Kooperman, G. J., Pritchard, M. S., Ghan, S. J., Wang, M., Somerville, R. C. J., and Russell, L. M.: Constraining the influence of natural variability to improve estimates of global aerosol indirect effects in a nudged version of the Community Atmosphere Model 5, Journal of Geophysical Research: Atmospheres, 117, https://doi.org/10.1029/2012JD018588, d23204, 2012.

Koster, R. D., Dirmeyer, P. A., Guo, Z., Bonan, G., Chan, E., Cox, P., Gordon, C. T., Kanae, S., Kowalczyk, E., Lawrence, D., Liu, P., Lu, C.-H., Malyshev, S., McAvaney, B., Mitchell, K., Mocko, D., Oki, T., Oleson, K., Pitman, A., Sud, Y. C., Taylor, C. M., Verseghy, D., Vasic, R., Xue, Y., and Yamada, T.: Regions of strong coupling between soil moisture and precipitation, Science, 305, 1138–1140, https://doi.org/10.1126/science.1100217, 2004.

Koster, R. D., Guo, Z., Yang, R., Dirmeyer, P. A., Mitchell, K., and Puma, M. J.: On the nature of soil moisture in land surface models, Journal of Climate, 22, 4322–4335, https://doi.org/10.1175/2009JCLI2832.1, 2009.

Lawrence, D. M., Oleson, K. W., Flanner, M. G., Thornton, P. E., Swenson, S. C., Lawrence, P. J., Zeng, X., Yang, Z.-L., Levis, S., Sakaguchi, K., Bonan, G. B., and Slater, A. G.: Parameterization improvements and functional and structural advances in version 4 of the Community Land Model, Journal of Advances in Modeling Earth Systems, 3, https://doi.org/10.1029/2011MS00045, 2011.

Maraun, D., Shepherd, T. G., Widmann, M., Zappa, G., Walton, D., Gutiérrez, J., Hagemann, S., Richter, I., Soares, P. M. M., Hall, A., and Mearns, L. O.: Towards process-informed bias correction of climate change simulations, Nature Climate Change, 7, 764–773, https://doi.org/10.1038/nclimate3418, 2017.

Mauritsen, T., Stevens, B., Roeckner, E., Crueger, T., Esch, M., Giorgetta, M., Haak, H., Jungclaus, J., Klocke, D., Matei, D., Mikolajewicz, U., Notz, D., Pincus, R., Schmidt, H., and Tomassini, L.: Tuning the climate of a global model, Journal of Advances in Modeling Earth Systems, 4, https://doi.org/10.1029/2012MS000154, 2012.

Meinshausen, M., Nicholls, Z. R. J., Lewis, J., Gidden, M. J., Vogel, E., Freund, M., Beyerle, U., Gessner, C., Nauels, A., Bauer, N., Canadell, J. G., Daniel, J. S., John, A., Krummel, P. B., Luderer, G., Meinshausen, N., Montzka, S. A., Rayner, P. J., Reimann, S., Smith, S. J., van den Berg, M., Velders, G. J. M., Vollmer, M. K., and Wang, R. H. J.: The shared socio-economic pathway (SSP) greenhouse gas concentrations and their extensions to 2500, Geoscientific Model Development, 13, 3571–3605, https://doi.org/10.5194/gmd-13-3571-2020, 2020.

550   Merz, B., Kuhlicke, C., Kunz, M., Pittore, M., Babeyko, A., Bresch, D. N., Domeisen, D. I. V., Feser, F., Koszalka, I., Kreibich, H., Pantillon, F., Parolai, S., Pinto, J. G., Punge, H. J., Rivalta, E., Schröter, K., Strehlow, K., Weisse, R., and Wurpts, A.: Impact forecasting to support emergency management of natural hazards, Reviews of Geophysics, 58, e2020RG000 704, https://doi.org/10.1029/2020RG000704, 2020.

Miralles, D. G., van den Berg, M. J., Teuling, A. J., and de Jeu, R. A. M.: Soil moisture-temperature coupling: a multiscale observational analysis, Geophysical Research Letters, 39, https://doi.org/10.1029/2012GL053703, 2012.

555   Miralles, D. G., Gentine, P., Seneviratne, S. I., and Teuling, A. J.: Land–atmospheric feedbacks during droughts and heatwaves: state of the science and current challenges, Annals of the New York Academy of Sciences, 1436, 19–35, https://doi.org/10.1111/nyas.13912, 2019.

Moon, H., Gudmundsson, L., and Seneviratne, S. I.: Drought persistence errors in global climate models, Journal of Geophysical Research: Atmospheres, 123, 3483–3496, https://doi.org/10.1002/2017JD027577, 2018.

Moon, H., Guillod, B. P., Gudmundsson, L., and Seneviratne, S. I.: Soil moisture effects on afternoon precipitation occurrence in current
560   climate models, Geophysical Research Letters, 46, 1861–1869, https://doi.org/10.1029/2018GL080879, 2019.

Mueller, B. and Seneviratne, S. I.: Systematic land climate and evapotranspiration biases in CMIP5 simulations, Geophysical Research Letters, 41, 128–134, https://doi.org/10.1002/2013GL058055, 2014.

Mueller, B., Hirschi, M., Jimenez, C., Ciais, P., Dirmeyer, P. A., Dolman, A. J., Fisher, J. B., Jung, M., Ludwig, F., Maignan, F., Miralles, D. G., McCabe, M. F., Reichstein, M., Sheffield, J., Wang, K., Wood, E. F., Zhang, Y., and Seneviratne, S. I.: Benchmark
565   products for land evapotranspiration: LandFlux-EVAL multi-data set synthesis, Hydrology and Earth System Sciences, 17, 3707–3720, https://doi.org/10.5194/hess-17-3707-2013, 2013.

Neale, R. B., Chen, C.-C., Gettelman, A., Lauritzen, P. H., Park, S., Williamson, D. L., Conley, A. J., Garcia, R., Kinnison, D., Lamarque, J.-F., Marsh, D., Mills, M., Smith, A. K., Tilmes, S., Vitt, F., Morrison, H., Cameron-Smith, P., Collins, W. D., Iacono, M. J., Easter, R. C., Ghan, S. J., Liu, X., Rasch, P. J., and Taylor, M. A.: Description of the NCAR Community Atmosphere Model (CAM 5.0), Technical
570   report, National Center for Atmospheric Research. Boulder, Colorado, 2012.

NOAA Climate Prediction Center: Historical El Niño / La Niña episodes (1950-present) based on the Oceanic Niño Index, https://origin.cpc.ncep.noaa.gov/products/analysis_monitoring/ensostuff/ONI_v5.php, accessed 17 May 2021, 2021.

Oleson, K. W., Lawrence, D. M., Bonan, G. B., Flanner, M. G., Kluzek, E., Lawrence, P. J., Levis, S., Swenson, S. C., Thornton, P. E., Dai, A., Decker, M., Dickinson, R., Feddema, J., Heald, C. L., Hoffman, F., Lamarque, J.-F., Mahowald, N., Niu, G.-Y., Qian, T., Randerson,
575   J., Running, S., Sakaguchi, K., Slater, A., Stöckli, R., Wang, A., Yang, Z.-L., Zeng, X., and Zeng, X.: Technical description of version 4.0 of the Community Land Model (CLM), Technical report, National Center for Atmospheric Research. Boulder, Colorado, 2010.

Pfahl, S., O'Gorman, P. A., and Fischer, E. M.: Understanding the regional pattern of projected future changes in extreme precipitation, Nature Climate Change, 7, 423–427, https://doi.org/10.1038/nclimate3287, 2017.

Power, S. B. and Delage, F. P. D.: Setting and smashing extreme temperature records over the coming century, Nature Climate Change, 9,
580   529–534, https://doi.org/10.1038/s41558-019-0498-5, 2019.

Quesada, B., Vautard, R., Yiou, P., Hirschi, M., and Seneviratne, S. I.: Asymmetric European summer heat predictability from wet and dry southern winters and springs, Nature Climate Change, 2, 736–741, https://doi.org/10.1038/nclimate1536, 2012.

Rahmstorf, S. and Coumou, D.: Increase of extreme events in a warming world, Proceedings of the National Academy of Sciences, 108, 17 905–17 909, https://doi.org/10.1073/pnas.1101766108, 2011.

585   Rayner, N. A., Parker, D. E., Horton, E. B., Folland, C. K., Alexander, L. V., Rowell, D. P., Kent, E. C., and Kaplan, A.: Global analyses of sea surface temperature, sea ice, and night marine air temperature since the late nineteenth century, Journal of Geophysical Research: Atmospheres, 108, https://doi.org/10.1029/2002JD002670, 2003.

Rossow, W. B. and Schiffer, R. A.: Advances in Understanding Clouds from ISCCP, Bulletin of the American Meteorological Society, 80, 2261–2288, https://doi.org/10.1175/1520-0477(1999)080%3C2261%3AAIUCFI%3E2.0.CO;2, 1999.

590   Santanello, J. A., Dirmeyer, P. A., Ferguson, C. R., Findell, K. L., Tawfik, A. B., Berg, A., Ek, M., Gentine, P., Guillod, B. P., van Heerwaarden, C., Roundy, J., and Wulfmeyer, V.: Land-atmosphere interactions: the LoCo perspective, Bulletin of the American Meteorological Society, 99, 1253–1272, https://doi.org/10.1175/BAMS-D-17-0001.1, 2018.

Seneviratne, S. I., Lüthi, D., Litschi, M., and Schär, C.: Land-atmosphere coupling and climate change in Europe, Nature, 443, 205–209, https://doi.org/10.1038/nature05095, 2006.

595   Seneviratne, S. I., Corti, T., Davin, E. L., Hirschi, M., Jaeger, E. B., Lehner, I., Orlowsky, B., and Teuling, A. J.: Investigating soil moisture-climate interactions in a changing climate: A review, Earth-Science Reviews, 99, 125–161, https://doi.org/10.1016/j.earscirev.2010.02.004, 2010.

Seneviratne, S. I., Nicholls, N., Easterling, D., Goodess, C. M., Kanae, S., Kossin, J., Luo, Y., Marengo, J., Innes, K. M., Rahimi, M., Reichstein, M., Sorteberg, A., Vera, C., Zhang, X., Rusticucci, M., Semenov, V., Alexander, L. V., Allen, S., Benito, G., Cavazos, T.,

600   Clague, J., Conway, D., Della-Marta, P. M., Gerber, M., Gong, S., Goswami, B. N., Hemer, M., Huggel, C., den Hurk, B. V., Kharin, V. V., Kitoh, A., Tank, A. M. G. K., Li, G., Mason, S., Guire, W. M., Oldenborgh, G. J. V., Orlowsky, B., Smith, S., Thiaw, W., Velegrakis, A., Yiou, P., Zhang, T., Zhou, T., and Zwiers, F. W.: Changes in climate extremes and their impacts on the natural physical environment, in: Managing the Risks of Extreme Events and Disasters to Advance Climate Change Adaptation, pp. 109–230, edited by C. B. Field et al., Cambridge University Press, Cambridge, https://doi.org/10.1017/CBO9781139177245.006, 2012.

605   Seneviratne, S. I., Donat, M. G., Mueller, B., and Alexander, L. V.: No pause in the increase of hot temperature extremes, Nature Climate Change, 4, 161–163, https://doi.org/10.1038/nclimate2145, 2014.

Shepherd, T. G.: Atmospheric circulation as a source of uncertainty in climate change projections, Nature Geosci, 7, 703–708, https://doi.org/10.1038/ngeo2253, 2014.

Shiogama, H., Watanabe, M., Imada, Y., Mori, M., Ishii, M., and Kimoto, M.: An event attribution of the 2010 drouwght in the South Amazon

610   region using the MIROC5 model, Atmospheric Science Letters, 14, 170–175, https://doi.org/10.1002/asl2.435, 2013.

Shiogama, H., Imada, Y., Mori, M., Mizuta, R., Stone, D., Yoshida, K., Arakawa, O., Ikeda, M., Takahashi, C., Arai, M., Ishii, M., Watanabe, M., and Kimoto, M.: Attributing historical changes in probabilities of record-breaking daily temperature and precipitation extreme events, Scientific Online Letters on the Atmosphere, 12, 225–231, 2016.

Sillmann, J., Kharin, V. V., Zwiers, F. W., Zhang, X., and Bronaugh, D.: Climate extremes indices in the CMIP5 multimodel ensemble: Part

615   2. Future climate projections, Journal of Geophysical Research: Atmospheres, 118, 2473–2493, https://doi.org/10.1002/jgrd.50188, 2013.

Takata, K., Emori, S., and Watanabe, T.: Development of the minimal advanced treatments of surface interaction and runoff, Global and Planetary Change, 38, 209–222, https://doi.org/10.1016/S0921-8181(03)00030-4, 2003.

Teng, H., Branstator, G., Tawfik, A. B., and Callaghan, P.: Circumglobal response to prescribed soil moisture over North America, Journal of Climate, 32, 4525–4545, https://doi.org/10.1175/JCLI-D-18-0823.1, 2019.

Earth System
Dynamics

Discussions

620 Trenberth, K. E., Fasullo, J. T., and Shepherd, T. G.: Attribution of climate extreme events, Nature Climate Change, 5, https://doi.org/10.1038/nclimate2657, 2015.

Turner, J., Bracegirdle, T. J., Phillips, T., Marshall, G. J., and Hosking, J. S.: An initial assessment of Antarctic sea ice extent in the CMIP5 models, Journal of Climate, 26, 1473–1484, https://doi.org/10.1175/JCLI-D-12-00068.1, 2013.

van der Ent, R. J., Savenije, H. H. G., Schaefli, B., and Steele-Dunne, S. C.: Origin and fate of atmospheric moisture over continents, Water

625 Resources Research, 46, https://doi.org/10.1029/2010WR009127, 2010.

van Vuuren, D. P., Edmonds, J., Kainuma, M., Riahi, K., Thomson, A., Hibbard, K., Hurtt, G. C., Kram, T., Krey, V., Lamarque, J.-F., Masui, T., Meinshausen, M., Nakicenovic, N., Smith, S. J., and Rose, S. K.: The representative concentration pathways: An overview, Climatic Change, 109, https://doi.org/10.1007/s10584-011-0148-z, 2011.

Vautard, R., Yiou, P., Otto, F., Stott, P., Christidis, N., van Oldenborgh, G. J., and Schaller, N.: Attribution of human-induced dynamical and

630 thermodynamical contributions in extreme weather events, Environmental Research Letters, 11, 114 009, https://doi.org/10.1088/1748-9326/11/11/114009, 2016.

Wang, C., Zhang, L., Lee, S.-K., Wu, L., and Mechoso, C. R.: A global perspective on CMIP5 climate model biases, Nature Clim. Change, 4, 201–205, https://doi.org/10.1038/nclimate2118, 2014.

Watanabe, M., Suzuki, T., O'ishi, R., Komuro, Y., Watanabe, S., Emori, S., Takemura, T., Chikira, M., Ogura, T., Sekiguchi, M., Takata, K.,

635 Yamazaki, D., Yokohata, T., Nozawa, T., Hasumi, H., Tatebe, H., and Kimoto, M.: Improved climate simulation by MIROC5: mean states, variability, and climate sensitivity, Journal of Climate, 23, 6312–6335, https://doi.org/10.1175/2010JCLI3679.1, 2010.

Wehrli, K., Guillod, B. P., Hauser, M., Leclair, M., and Seneviratne, S. I.: Assessing the dynamic versus thermodynamic origin of climate model biases, Geophysical Research Letters, 45, 8471–8479, https://doi.org/10.1029/2018GL079220, 2018.

Wehrli, K., Guillod, B. P., Hauser, M., Leclair, M., and Seneviratne, S. I.: Identifying key driving processes of major recent heat waves,

640 Journal of Geophysical Research: Atmospheres, 124, 11 746–11 765, https://doi.org/10.1029/2019JD030635, 2019.

Wehrli, K., Hauser, M., and Seneviratne, S. I.: Storylines of the 2018 Northern Hemisphere heatwave at pre-industrial and higher global warming levels, Earth System Dynamics, 11, 855–873, https://doi.org/10.5194/esd-11-855-2020, 2020.

Zappa, G., Shaffrey, L. C., and Hodges, K. I.: The ability of CMIP5 models to simulate North Atlantic extratropical cyclones, Journal of Climate, 26, 5379–5396, https://doi.org/10.1175/JCLI-D-12-00501.1, 2013.

645 Zappa, G., Hoskins, B. J., and Shepherd, T. G.: The dependence of wintertime Mediterranean precipitation on the atmospheric circulation response to climate change, Environmental Research Letters, 10, 104 012, https://doi.org/10.1088/1748-9326/10/10/104012, 2015.

Ziese, M., Rauthe-Schöch, A., Becker, A., Finger, P., Meyer-Christoffer, A., and Schneider, U.: GPCC Full Data Daily Version.2018 at 1.0°: daily land-surface precipitation from rain-gauges built on GTS-based and historic data, https://doi.org/10.5676/dwd_gpcc/fd_d_v2018_100, 2018.

650 Zscheischler, J. and Seneviratne, S. I.: Dependence of drivers affects risks associated with compound events, Science Advances, 3, https://doi.org/10.1126/sciadv.1700263, 2017.